ISSN 2830-9820

Visual Computing MAGAZiNE

Vol. 1, Issue 3
2023

AI and AR for Medical Imaging

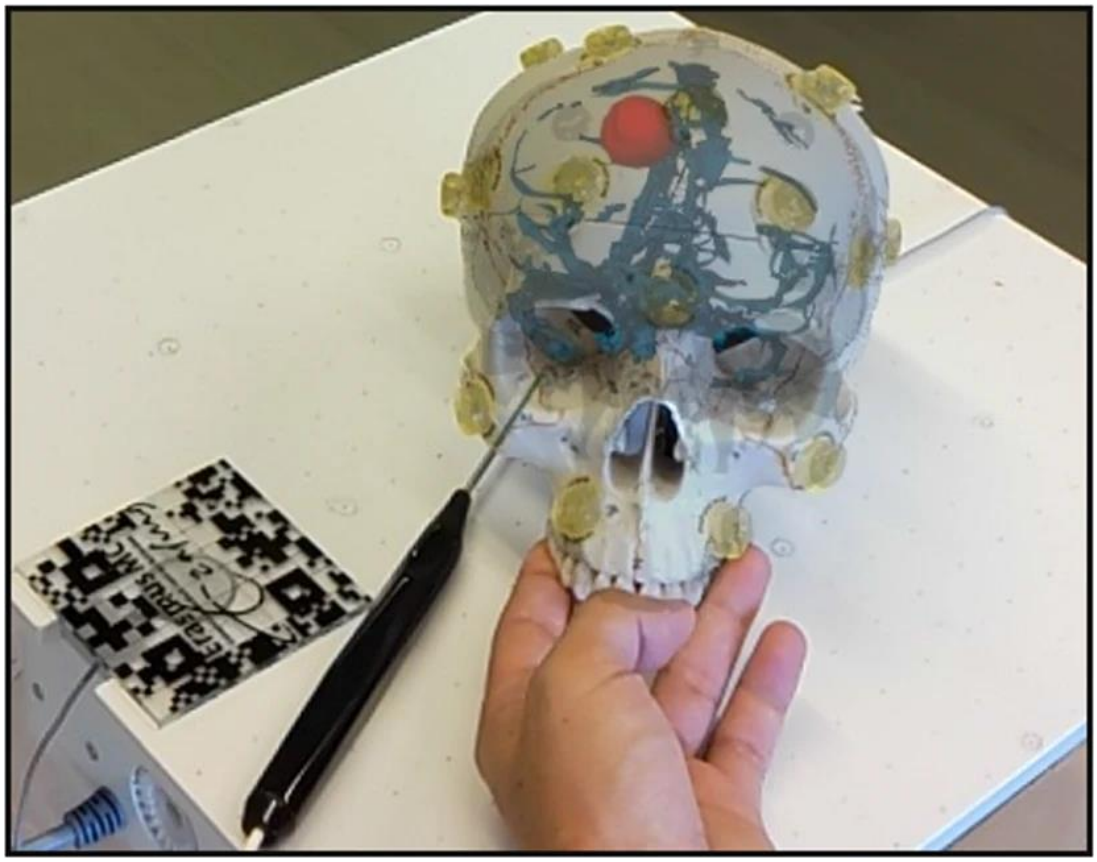

Deep Learning-Based Mitosis Detection in Breast Cancer Histopathology Images

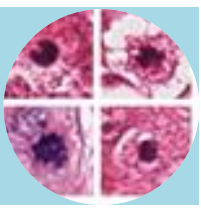

The Foreword

Welcome to the third issue of Visual Computing Magazine. In this issue, we are delighted to present two invited papers related to medical imaging.

Medical imaging, until 10 years ago, was a field in which smart researchers and engineers developed a multitude of advanced methods for automatic segmentation and registration of medical images. Examples of these approaches are levelsets and graph cuts for segmentation, diffusion algorithms for image enhancement, active shape and appearance models to integrate population statistics in segmentation approaches, and a large variety of registration approaches, where optimizers, cost functions and transformation models have been investigated. This has changed dramatically the last decade, because of the introduction of AI in medical imaging. The introduction of U-Net to the field, at MICCAI 2015 in Munich, can be seen as the start of this change. Since then, the AI started to take off, with more than 70 % of deep learning papers already at MICCAI 2018. The good thing about this change is that the field now has much more effective tools to address the imaging challenges at hand. An example here is nnU-net (Isensee et al.), which now allows even non-imaging specialists to create effective segmentation approaches, provided that good training data can be constructed. The implication for the medical imaging field is that we can focus on more complex challenges. In addition, there is more potential of bringing effective approaches to clinical translation. The mitosis detection in breast cancer is a good example of the possibilities of the opportunities that this paradigm shift has brought us.

In surgical navigation, a similar trend, though not as profound, can be witnessed. Navigation approaches have become standard for e.g., neurosurgical and orthopedic procedures. During the navigation, pre-operative imaging and planning is aligned with the patient, and subsequently the instruments can be visualized, together with planning and pre-operative imaging, on a 2D screen. These approaches allow surgeons to do advanced procedures, that may not be possible using eye-sight only. Whereas powerful, the application of these systems still is hampered by the advanced technology required, the cumbersome step of aligning the images, and the 2D visualization which is not always aligned with the surgeon's view on the patient. The introduction of see-through augmented reality devices, such as HoloLens 1 and 2 and Magic Leap, has started several groups to investigate approaches to integrate the augmented reality in navigation, or even using such devices for stand-alone navigation, and using the sensors of these devices to simplify image-to-patient registration. These approaches are not as sophisticated as their AI counterparts yet, it is however expected that the further introduction of augmented reality in surgical navigation may improve both the usability of current navigation approaches, and enable navigation in procedures that are now done without navigation. The manuscript on AR for Medical Imaging is a thorough introduction to the techniques that are involved in this transition.

Dr. Ir. Theo Van Walsum
Principal Investigator
Department Radiology & Nuclear Medicine
Erasmus MC, University Rotterdam, the Netherlands

Visual Computing: A quarterly magazine. Volume 1, Issue 3, 2023
***ISSN:* 2830-9820**
Chief Editor: Prof. Slimane LARABI

Visual Computing Magazine

AR for Medical imaging

Mohamed Benmahdjoub, Thabit A., Wiro J. Niessen, Eppo B. Wolvius, Marie-Lise C. Van Veelen , Theo van Walsum, Biomedical Imaging Group Rotterdam, Erasmus MC, The Netherlands

1. Introduction

Medical imaging is the field that focuses on the acquisition and analysis of patient specific images acquired by scanner devices. These images can be acquired through various modalities such as the well-known X-ray, Ultrasound (US), Computed Tomography (CT), and Magnetic Resonance Imaging (MRI) [1] (See Fig. 1a and Fig. 1b).

These imaging modalities provide an inner visualization of the tissues or bony structures that are underneath the skin. Those modalities can acquire single 2D images, such as in the case of X-Ray and US images, or as a stack of 2D images which constitutes a 3D volume of the captured anatomy in the case of CT or MRI modalities.

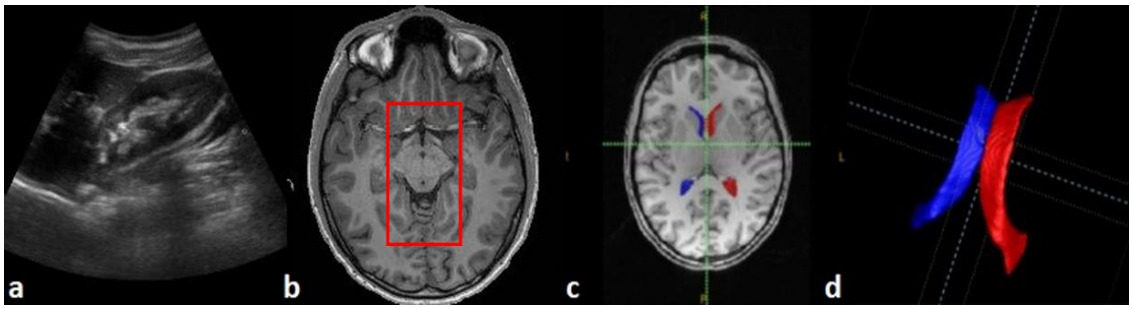

Figure 1. (a): Ultrasound liver scan [2], (b) MRI brain scan [3], (c) ventricles segmentation in a brain MRI image, (d) and 3D reconstruction of the ventricles from an MRI image [4].

The acquired images can be used as a diagnosis tool preoperatively, as a reference during surgery (perioperatively), or as a postoperative tool to evaluate the success of a surgical intervention.

To facilitate the previous tasks, various operations can be performed on the acquired images: detection, classification, segmentation and 3D reconstruction are the most common. For instance, the first one consists of locating brain ventricles (Fig. 1b), the second consists of identifying the type of disease in the image, the third one consists of identifying which part of the image (a group of pixels) represent a certain anatomy (Fig. 1c), and the last one consists of using the 2D stack of images to create a 3D reconstruction of the ventricles (Fig. 1d).

In the case where a surgical procedure is needed, these procedures allow for surgical planning. This procedure consists for instance of defining incision lines, plan drilling trajectories, plan trajectories to reach a target (e.g., tumor), planning implant shape based on the shape of the anatomy, etc.

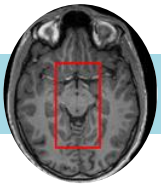

AR for Medical imaging

Mohamed Benmahdjoub, Thabit A., Wiro J. Niessen, Eppo B. Wolvius, Marie-Lise C. Van Veelen , Theo van Walsum, Biomedical Imaging Group Rotterdam, Erasmus MC, The Netherlands

However, to localize a tumor that was detected on medical images on the real surgical area, amidst blood and other organs, proves to be challenging and requires experience and adequate knowledge. This is where surgical navigation and image-guided interventions field comes in. This field focuses on the techniques (software/hardware) that would allow the mapping of the medical images and the surgical planning onto the surgical site, in other terms alignment/registration. This means that a surgeon will be capable of knowing where his surgical instruments and planning are with respect to the patient anatomy (patient space/patient's coordinate system). The devices enabling such features are called navigation systems. Conventionally, navigation systems consist of a tracking system, and a screen that allows for the visualization of medical data and the location of instruments in those images (see Fig. 2).

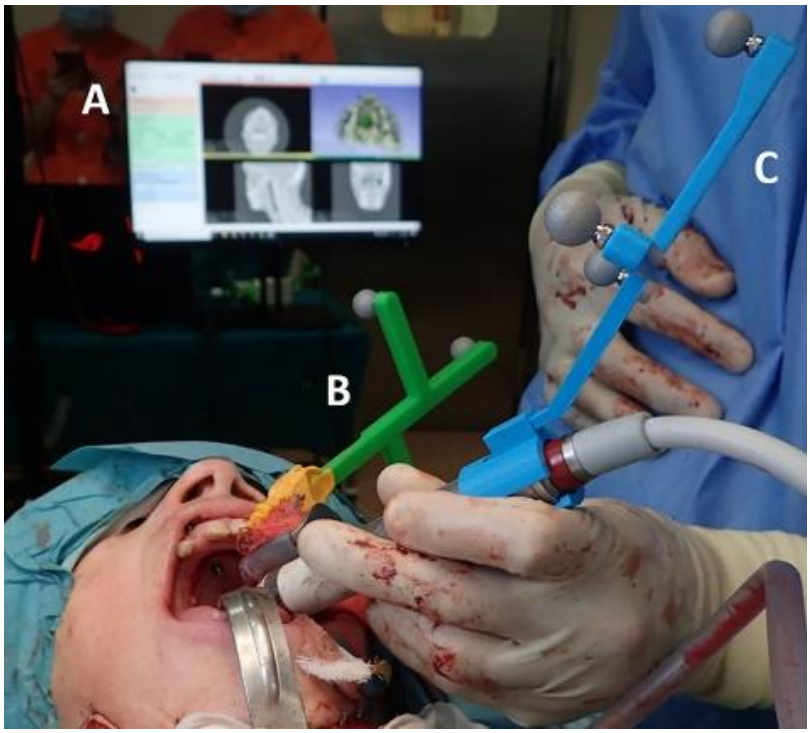

Figure 2. Example of a navigation system for surgery [5].

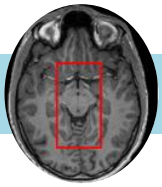

AR for Medical imaging

Mohamed Benmahdjoub, Thabit A., Wiro J. Niessen, Eppo B. Wolvius, Marie-Lise C. Van Veelen , Theo van Walsum, Biomedical Imaging Group Rotterdam, Erasmus MC, The Netherlands

2. Multimodal markers for augmented surgical navigation [6]

Image-to-patient alignment is a crucial procedure in surgical navigation. It registers/aligns patient data accurately on the target anatomy in terms of position and rotation. It enables surgeons to locate their surgical planning, and to determine where their instruments are located with respect to the patient's anatomy. Using conventional navigation systems, surgeons need to provide two corresponding sets of points of anatomical landmarks on the patient, by using a tracked pointer for example, and on the patient data's coordinate system (e.g., CT or MRI). Subsequently, the transformation matrix from the patient's coordinate system to the real world is computed.

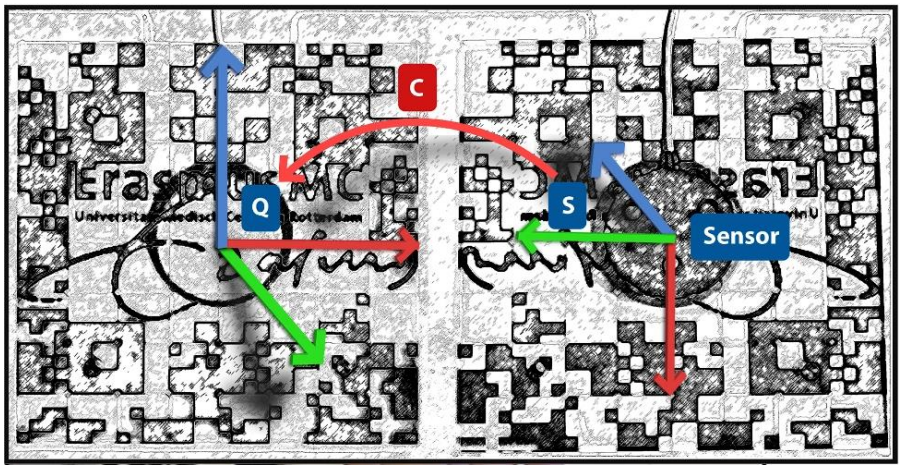

Figure 3. Multimodal marker, Q: 2D pattern coordinate system, S: Electromagnetic sensor's coordinate system, C: The calibration matrix between S and Q.

In an augmented reality (AR) context, image-to-patient alignment is the process that allows to tell the AR device, for e.g., head-mounted displays (HMD) such as the Microsoft HoloLens 2, where the patient is located in 3D space with respect to the user. A common approach in the literature to align a 3D patient model with the patient, is to attach rigidly a 2D pattern (e.g., QR code) on the patient's anatomy (e.g., teeth) based on the CT image at a known location, and estimate its pose [7]. However, this approach requires the printing of 2D patterns for every patient. Therefore, extending preparation times (e.g., sterilization), which is not suitable for trauma cases. Another approach is to attach markers such as reflective spheres (see Fig. 2 B) on the HMD, this way, the conventional navigation system is able to locate the patient, the instruments and the device in the same coordinate system. This approach requires the calibration of every new HMD with the external tracking system, and oblige surgeons to stay within a specific field of view of the tracking system [8].

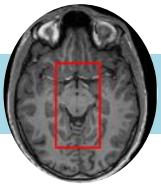

AR for Medical imaging

Mohamed Benmahdjoub, Thabit A., Wiro J. Niessen, Eppo B. Wolvius, Marie-Lise C. Van Veelen , Theo van Walsum, Biomedical Imaging Group Rotterdam, Erasmus MC, The Netherlands

We proposed a solution using a multimodal marker, which is made of a 2D pattern on which a tracked marker is attached. Figure 3 shows an example of a multimodal marker where an electromagnetic sensor is attached to a 2D pattern. The latter is tracked by the HMD and the sensor is tracked by an electromagnetic tracking system (EMTS). A calibration matrix (C) is computed between the sensor and the 2D pattern. This transformation allows to link the coordinate systems of the HMD and the tracking system.

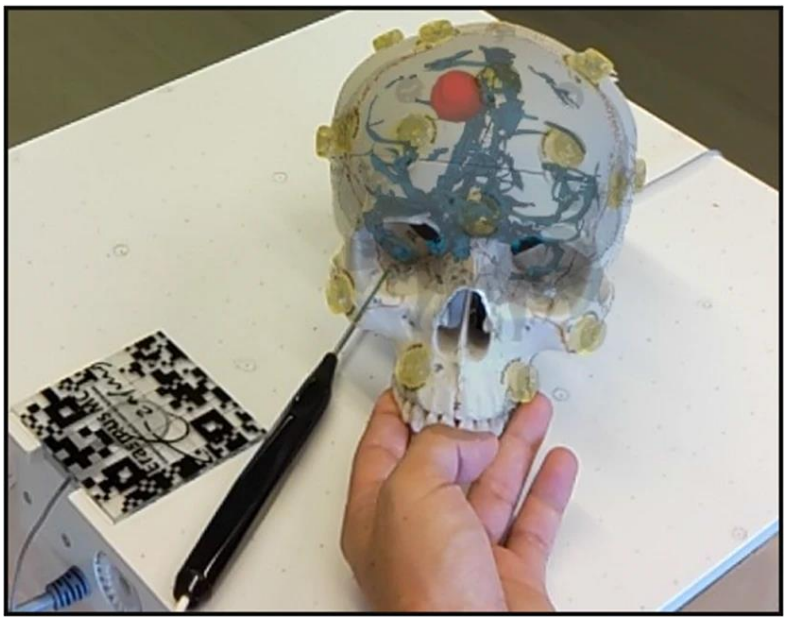

Figure 4. An AR view of a projected skull using the HoloLens 2 and a multimodal marker.

This developed approach allowed the projection of the 3D model of the skull (See Fig. 4) with a mean accuracy of 2.7 mm which is an acceptable accuracy for some surgical interventions for instance in the case if craniosynostosis.

More investigations on marker size, number of markers, depth perception effect on surgical performance.

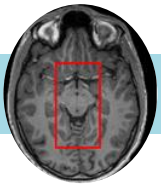

AR for Medical imaging

Mohamed Benmahdjoub, Thabit A., Wiro J. Niessen, Eppo B. Wolvius, Marie-Lise C. Van Veelen , Theo van Walsum, Biomedical Imaging Group Rotterdam, Erasmus MC, The Netherlands

3. Virtual extensions improve perception-based instrument alignment using optical see-through devices [9]

Instrument alignment is a common task performed by surgeons when drilling, or inserting a needle to reach a target anatomy. Surgeons would follow a specific preplanned trajectory and align their surgical instrument with it. The need for accurate placement of an instrument in surgical tasks is crucial for the safety of the patient. In augmented reality (AR), it is difficult to perceive the exact location (position and orientation) of a preplanned trajectory visualized as a cylinder. It has been reported in the literature that users performing matching and reaching tasks, find it difficult to estimate depth, especially when using optical see-through (OST) devices (e.g., Microsoft HoloLens). In fact, users tend to underestimate the depth of the projected virtual models i.e., the distance from the user to virtual content [10].
In this study, we evaluate three visualization paradigms on an instrument alignment task in AR when using the OST device HoloLens 2. In the first visualization, only the preplanned trajectory is visualized (Fig. 5 left). In the second visualization, both the preplanned trajectory and a realistic visualization of the instrument are projected (Fig. 5 middle). In the third visualization, we introduce the paradigm of virtual extensions where we attach virtual 3D objects (disks) to both the preplanned trajectory and the instrument (Fig. 5 right).

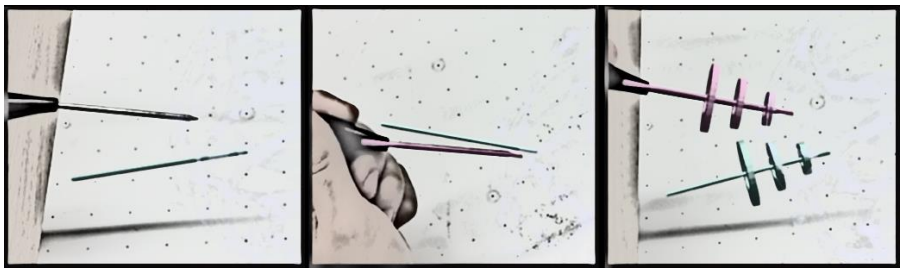

Figure 5. Instrument alignment with a pre-planned trajectory (cyan) under various conditions. Left: No instrument visualization.

18 volunteers participated in this study, where they were asked to perform the alignment task and the tip-to-tip distance and angle between the instrument and the preplanned trajectory was computed. Users performed the best under the virtual extensions paradigm with 2 mm distance and 1.8° compared to the realistic visualization and no visualization of the instrument with 3.8 mm and 2.4°, and 10 mm and 4.4° respectively.

Virtual extensions improved the overall accuracy of all users, reduced their frustration levels and increased their confidence in the performed task. All of these results were reflected on the preference of users where half of the participants (9) appreciated the use of the virtual extensions. Therefore, this study showed the importance of surgical instruments visualization in AR, and proposed a new paradigm which proved to be useful for an accurate alignment.

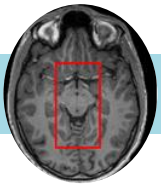

AR for Medical imaging

Mohamed Benmahdjoub, Thabit A., Wiro J. Niessen, Eppo B. Wolvius, Marie-Lise C. Van Veelen , Theo van Walsum, Biomedical Imaging Group Rotterdam, Erasmus MC, The Netherlands

4. Towards AR-guided craniosynostosis surgery [11]

Craniosynostosis is a congenital disease in which the skull bones of a baby are joint prematurely. This results in a deformed growth of the skull causing intracranial pressure. This can lead to several health complications such as blindness, seizures or brain damage [12]. The most prevalent type of craniosynostosis is sagittal synostosis which occurs in 40–60% of the single suture synostosis cases and which results in an elongated shape of the head (see Fig. 6).

Generally, a surgical procedure is required to correct for this abnormal growth. It is done by performing a complete remodeling of the skull, or by conducting minimally invasive procedures such as spring-assisted craniectomy which is known to reduce blood loss during the intervention [13].
In spring-assisted craniectomy, surgeons try to feel anatomical sutures with their hands (coronal, lambdoid and sagittal), and based on that, they draw where incision lines should be. These cranial sutures are sometimes hard to feel because of the presence of hair and skin, resulting in a shift of 10-20mm of the preplanned incision lines.
Augmented reality (AR) could be an alternative to this free-hand approach, by providing a visualization of the cranial sutures and/or the incision lines.

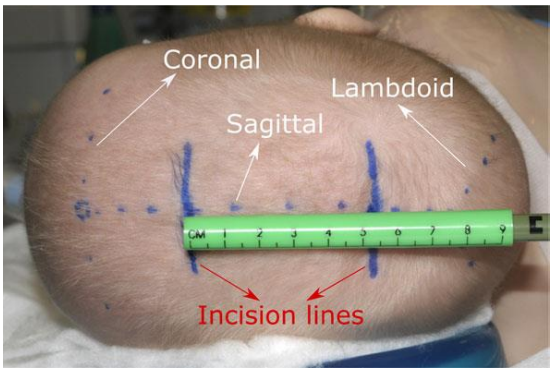

Figure 6. Surgery planning in minimally invasive spring-assisted craniectomy, showing the coronal, lambdoid and sagittal sutures marked by the surgeon, as well as the planned incisions [13]

We investigated the use of AR of this intervention by conducting a user study where 12 volunteers with various backgrounds participated. The AR system previously developed [13], was used to project and visualize CT annotated cranial sutures on a 3D printed skull (See Fig. 7). The participants were asked to delineate the location of these sutures with a pen, and we computed its accuracy by using an optical tracking system (NDI Vega). The distance between the CT annotated sutures and the drawn sutures resulted in an average accuracy of ~ 2 mm for the coronal suture and 3.3 mm for lambdoid suture.

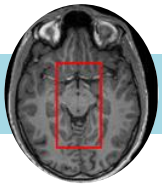

AR for Medical imaging

Mohamed Benmahdjoub, Thabit A., Wiro J. Niessen, Eppo B. Wolvius, Marie-Lise C. Van Veelen , Theo van Walsum, Biomedical Imaging Group Rotterdam, Erasmus MC, The Netherlands

This study showed an acceptable accuracy using AR compared to the free-hand approach. Therefore, there is a potential for AR to enable surgical navigation for craniosynostosis surgery.

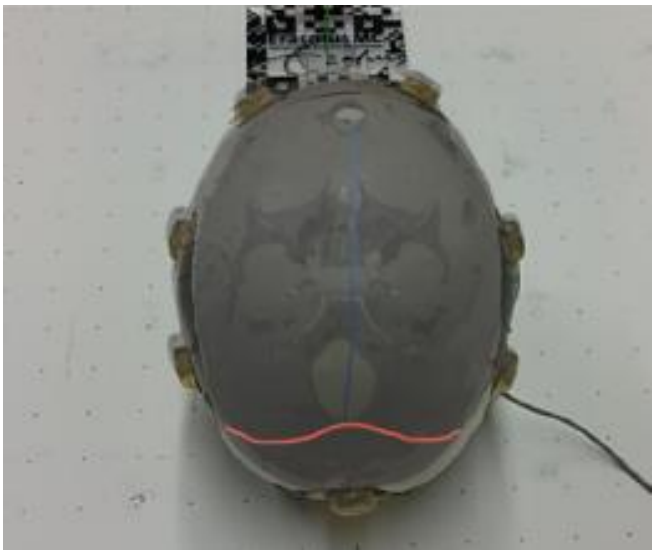

Figure 7. Cranial sutures visualized through the HoloLens 2 for the users to delineate.

5. 3D vs. 2D AR visualization for surgical navigation [14]

Hydrocephalus is a condition where the cerebrospinal fluid (CSF) is accumulated inside the brain ventricles which enlarges them (see Fig. 8). This can cause brain intracranial pressure leading to several health complications [15]. An external ventricular drain (EVD) procedure is generally performed as a temporary solution to release the CSF from the ventricles. This intervention consists of inserting a drain inside the right ventricle, to extract any excess of the CSF. The insertion is generally performed blindly by relying on head measurements (see Fig. 8). However, in a previous study, 23% misplacement occurred in which 40% required reinsertion of the catheter [16].

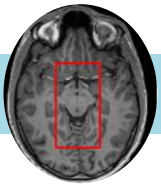

AR for Medical imaging

Mohamed Benmahdjoub, Thabit A., Wiro J. Niessen, Eppo B. Wolvius, Marie-Lise C. Van Veelen , Theo van Walsum, Biomedical Imaging Group Rotterdam, Erasmus MC, The Netherlands

This study showed an acceptable accuracy using AR compared to the free-hand approach. Therefore, there is a potential for AR to enable surgical navigation for craniosynostosis surgery.

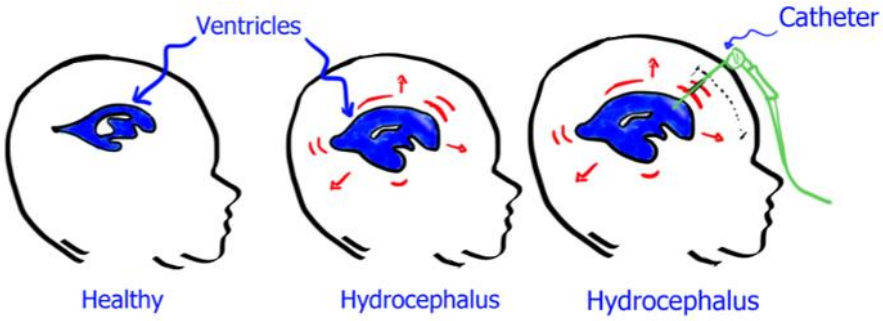

Figure 8. Hydrocephalus and catheter placement in EVD.

Augmented reality (AR) could project ventricles on top of the patient to assist the surgeon.
Several visualization approaches in AR have been proposed in the literature. This study, investigated the adequate visualization for EVD surgical navigation using 3D vs. 2D AR approaches (see Fig. 9).

32 volunteers participated in this study. Their task was to insert a tracked needle inside a phantom skull which contained gelatin to simulate the properties of soft tissue. The needle had to be placed exactly matching the preplanned trajectory shown inside the skull. The results from this study showed a higher performance using 3D approaches in terms of accuracy (~2 mm, ~1.5°), and in terms of user preference. These results provide more evidence and incentive for surgeons to use a stereoscopic head-mounted display instead of a 2D screen for surgical navigation.

Figure 9. The AR visualization approaches compared in the study. In orange, 2D visualization approaches: smartphone, and a 2D navigation window visualized through the HoloLens. In purple, 3D visualization approaches through the HoloLens: fully aligned model on the phantom skull, and shifted model with rotations aligned with the phantom's rotations.

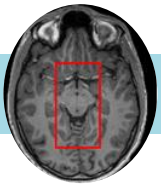

AR for Medical imaging

Mohamed Benmahdjoub, Thabit A., Wiro J. Niessen, Eppo B. Wolvius, Marie-Lise C. Van Veelen , Theo van Walsum, Biomedical Imaging Group Rotterdam, Erasmus MC, The Netherlands

Conclusion (AR & surgical navigation)

AR allows to combine data from medically acquired images as 3D reconstructed models. These models are projected on top of the patient by the AR device (e.g., head-mounted displays). It provides the surgeon with a see-through visualization of the underlying anatomy of the patient. The surgeon can include steps of the surgical procedure, including for example drilling and insertion trajectories, to reach the preplanned outcome. AR can become a mainstream navigation technology for currently non-navigated surgical interventions, and enable increased precision and improved surgical outcomes. AR for surgical navigation could mitigate under staffing in hospitals where experienced surgeons are lacking. Indeed, AR navigation could provide assistance to less experienced surgeons in performing similarly to experienced surgeons.

However, a few challenges are still open to be addressed, including accurate image-to-patient alignment, continuous tracking, depth perception in AR and clinical translation to the operating room (OR), which require more improvements on both current hardware and software solutions.

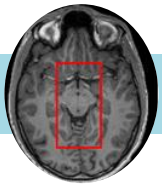

AR for Medical imaging

Mohamed Benmahdjoub, Thabit A., Wiro J. Niessen, Eppo B. Wolvius, Marie-Lise C. Van Veelen , Theo van Walsum, Biomedical Imaging Group Rotterdam, Erasmus MC, The Netherlands

References

[1] Bushberg, J. et al., (2011). The essential physics of medical imaging (3rd ed.). Lippincott Williams and Wilkins.
[2] https://www.kaggle.com/datasets/ignaciorlando/ussimandsegm?resource=download
[3] Eichhorn H. et al. Evaluating the performance of markerless prospective motion correction and selective reacquisition in a general clinical protocol for brain MRI n.d. Doi: 10.31234/OSF.IO/VZH4G.
[4] https://en.wikipedia.org/wiki/File:Itksnapsshot.png
[5] García-Sevilla M., et al. Surgical Navigation, Augmented Reality, and 3D Printing for Hard Palate Adenoid Cystic Carcinoma En-Bloc Resection: Case Report and Literature Review. Front Oncol 2022;11:741191. Doi: 10.3389/FONC.2021.741191/BIBTEX.
[6] Benmahdjoub, M., Niessen, W.J., Wolvius, E.B. et al. Multimodal markers for technology-independent integration of augmented reality devices and surgical navigation systems. Virtual Reality 26, 1637–1650 (2022). https://doi.org/10.1007/s10055-022-00653-3
[7] Benmahdjoub M., Niessen WJ., Wolvius EB., Van Walsum T. Virtual extensions improve perception-based instrument alignment using optical see-through devices. IEEE Trans Vis Comput Graph 2021;27(11):4332–41. Doi: 10.1109/TVCG.2021.3106506.
[8] Jiang, T., Zhu, M., Chai, G. et al. Precision of a Novel Craniofacial Surgical Navigation System Based on Augmented Reality Using an Occlusal Splint as a Registration Strategy. Sci Rep 9, 501 (2019). https://doi.org/10.1038/s41598-018-36457-2
[9] Benmahdjoub M, Niessen WJ, Wolvius EB, van Walsum T. Virtual extensions improve perception-based instrument alignment using optical see-through devices. IEEE Trans Vis Comput Graph. 2021 Nov;27(11):4332-4341. doi: 10.1109/TVCG.2021.3106506. Epub 2021 Nov 2. PMID: 34449385.
[10] Gurjot Singh, J. Edward Swan, J. Adam Jones, Stephen R. Ellis. Depth judgment measures and occluding surfaces in near-field augmented reality. APGV '10: Proceedings of the 7th Symposium on Applied Perception in Graphics and VisualizationJuly 2010Pages 149–156https://doi.org/10.1145/1836248.1836277.
[11] Thabit A., Benmahdjoub M., van Veelen MLC., Niessen WJ., Wolvius EB., van Walsum T. Augmented reality navigation for minimally invasive craniosynostosis surgery: a phantom study. Int J Comput Assist Radiol Surg 2022;17(8):1453–60. Doi: 10.1007/S11548-022-02634-Y/TABLES/5.
[12]https://www.cdc.gov/ncbddd/birthdefects/craniosynostosis.html#:~:text=Craniosynostosis%20is%20a%20birth%20defect,skull%20can%20become%20more%20misshapen
[13] van Veelen M-LC, Mathijssen IM (2012) Spring-assisted correction of sagittal suture synostosis. Childs Nerv Syst 28(9):1347–1351
[14] Benmahdjoub M., Thabit A., van Veelen MLC., Niessen WJ., Wolvius EB., Walsum T van. Evaluation of AR visualization approaches for catheter insertion into the ventricle cavity. IEEE Trans Vis Comput Graph 2023;(01):1–12. Doi: 10.1109/TVCG.2023.3247042.
[15] H. M. Tully and W. B. Dobyns. Infantile hydrocephalus: a review of epidemiology, classification and causes. European journal of medical genetics, 57(8):359–368, 2014.
[16] Toma AK, Camp S, Watkins LD, Grieve J, Kitchen ND (2009) External ventricular drain insertion accuracy: is there a need for change in practice? Neurosurgery 65:1197–1201

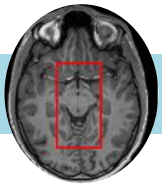

Visual Computing Magazine

Toward accurate deep learning-based mitosis detection in breast cancer histopathology images

Meriem Sebai. Computer Science Faculty, Algeria
Xinggang Wang, Tianjiang Wang. Huazhong University of Science and Technology (HUST), Wuhan, People's Republic of China
S. A. Al-Fadhli. Imam Al-Kadhum College (IKC), Baghdad, Iraq

Abstract

The detection and counting of mitotic cells on the histology slides is the most crucial indicator of tumour grade in the prognosis of breast cancer. The detection of mitotic cells is usually performed manually by a pathologist under a microscope, which is a very tedious task, and the development of an accurate automatic mitosis detection method is therefore extremely valuable for pathology practice.

We propose three novel convolutional neural network (CNN)-based methods for the automatic mitosis detection. Most of the existing methods perform mitosis detection using classification, regression, or object detection task. These methods suffer from several drawbacks in terms of their accuracy and reliability, due to the appearance variations of the mitotic cells and the similarity between them and other cells. In the proposed work, we assume that performing mitosis segmentation is the key step in order to better capture the complex shape and appearance characteristics of the mitotic cells. Hence, all of the three proposed methods involve a procedure of mitosis segmentation. To attain full supervision information to train a segmentation-based method for mitosis detection, mitosis pixel-level labels are required. Since only a few datasets provide mitosis pixel-level annotations (i.e., strong labels), and the majority of the datasets only have mitosis centroid-pixel labels (i.e., weak labels), the main goal of this research work is to make each proposed framework able to learn from these weakly labelled data. For this purpose, we explore two major research areas in deep learning, which are weakly supervised learning and deep transfer learning. The weakly supervised learning is used to learn CNN-based models for mitosis detection under the weak supervision of mitosis centroid-pixel annotations, while the deep transfer learning is used to exploit the few available strongly labelled data to learn CNN-based models for mitosis detection on weakly labelled data.

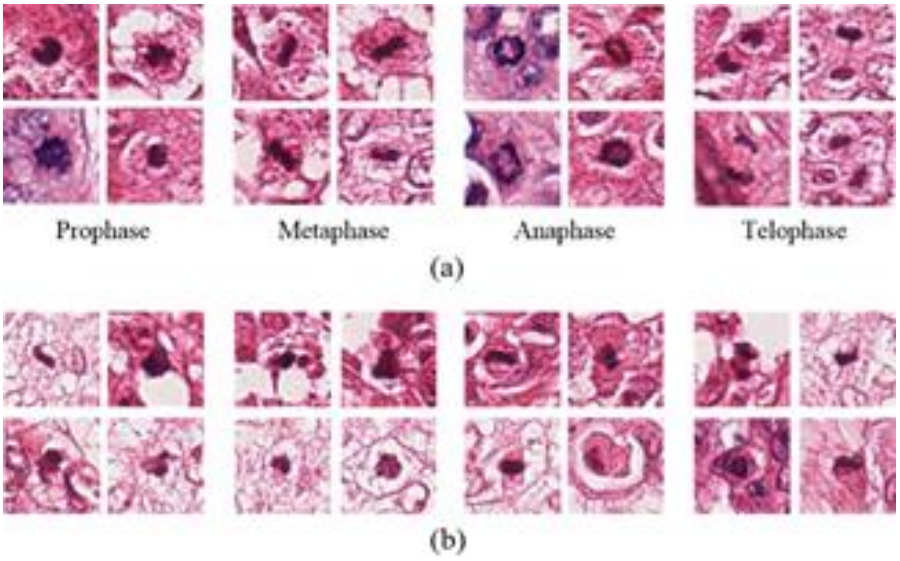

Figure 1. Samples of mitotic and non-mitotic cells: (a) mitotic cells in different growth stages; (b) non-mitotic mimic cells.

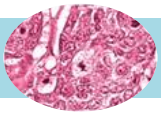

Visual Computing Magazine

Toward accurate deep learning-based mitosis detection in breast cancer histopathology images

Meriem Sebai. Computer Science Faculty, Algeria
Xinggang Wang , Tianjiang Wang. Huazhong University of Science and Technology (HUST), Wuhan, People's Republic of China
S. A. Al-Fadhli. Imam Al-Kadhum College (IKC), Baghdad, Iraq

1. Introduction

Microscopy image analysis in general, and histopathology image analysis in particular, form one of the most crucial quantitative pillars of the finer characterization of a diverse range of diseases, such as brain tumors, lung cancer, and breast cancer.
Breast cancer (BC) is the most commonly diagnosed cancer worldwide, and is the primary cause of cancer mortality among women [1]. A histologic grading system is used to define how aggressively a breast tumour can behave. The tumour is analysed by observing the cancer cells under a microscope and describing the abnormalities in their appearance. This provides an estimation of the potential spread of cancer and a probability of distant metastasis, and thus helps in the selection of high-risk treatments [2].
Various scoring systems are available for the assessment of the histological grade of BC. One of the first was Greenough's 1925 grading system [3], which estimated the grade of invasive BC by quantifying seven biomarkers, which were later reduced to only three by Bloom and Richardson [4]. This system was officially approved and recommended by the World Health Organisation (WHO) after the Nottingham revision [5] (also called the Elston-Ellis modification) in 1991.

According to the Nottingham grading system (NGS) [5], expert pathologists should take into consideration the following three factors when grading BC: Tubule formation, nuclear pleomorphism, and mitotic activity and tumour proliferation. A score of 1–3 is assigned to each of these features. Tissues with a score of 1 are the closest to normal, while those with a score of 3 are the most abnormal. The three scores are summed to obtain the final Nottingham score of between 3 and 9. Each score is assigned to a corresponding grade, as follows: a low grade (grade I) is assigned to a Nottingham score of 3 to 5; an intermediate grade (grade II) is assigned to a Nottingham score of 6 or 7; and a high grade (grade III) is assigned to a Nottingham score of 8 or 9.

The growth rate or proliferation speed of a tumour is the most critical indicator in BC prognosis. It is commonly assessed based on its correlate at the cell level, the number of mitotic cells. This forms the main component of the NGS, the grading system used worldwide for BC prognosis, but it is also often considered to be an independent and self-sufficient prognosis factor for BC. Hence, in the prognosis of BC, estimations of mitotic activity are used in relation to different neoplasms, and those with higher proliferation (i.e., higher mitotic activity) generally have a worse prognosis.
Active cells pass through a process that can be divided into two main phases (interphase and the mitotic phase), known collectively as the cell cycle. In the mitotic phase, a cell reproduces in the form of two genetically identical daughter cells (i.e., two cells with the same numbers of chromosomes). This phase includes four stages of growth: the prophase, metaphase, anaphase, and telophase. Mitosis is a crucial biological process for life, as it allows for the production of new cells for growth and the replacement of worn-out cells. This mitosis process sometimes goes wrong, leading to the production of new abnormal cells, such as cells with extra chromosomes or deficiencies. These abnormal cells typically cannot support the life of a cell, and die; however, some manage to survive and proliferate. These cells are often implicated in cancer.

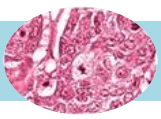

Toward accurate deep learning-based mitosis detection in breast cancer histopathology images

Meriem Sebai. Computer Science Faculty, Algeria
Xinggang Wang, Tianjiang Wang. Huazhong University of Science and Technology (HUST), Wuhan, People's Republic of China
S. A. Al-Fadhli. Imam Al-Kadhum College (IKC), Baghdad, Iraq

Mitotic cell detection (i.e., marking each mitotic cell with the nearest single point to its centroid) is performed by an expert pathologist based on a small, pre-selected region with an area of 2 mm2. This region is delimited from the whole slide image (WSI) at low microscope magnification as the highest cellularity area (i.e., the area with the highest mitotic activity) in the periphery of the tumour. In order to count the total number of mitotic cells, expert pathologists generally analyse the pre-selected region using 10 consecutive high-power fields (HPFs). An HPF is the area visible through a microscope at high magnification (generally 40×). Then, according to the number of mitotic cells in these 10 HPFs, a histological score of the mitotic activity is assigned.

Over the past decade, following the introduction of WSI scanners that allow for the full digitalisation of the pathology workflow and the representation of glass slides in digital format, the demand for the development of automated mitosis detection frameworks has become high in pathology laboratories, in order to aid pathologists in their work. Mitosis detection and counting is an extremely time-consuming and labour-intensive task, since the manual detection of mitoses from a single 2 mm2 area (i.e., 10 HPFs) may take between 5 and 10 minutes [6]. Moreover, although mitosis counting is routinely performed by pathologists in medical laboratories, problems arise with regard to reproducibility (especially among non-specialist pathologists), which are mainly caused by the subjectivity and the difficulty of the task. Therefore, the automation of the mitosis detection procedure will not only reduce the time and the labor required for mitosis detection in pathology laboratories, but will also help to consolidate the pathologists' decisions.

Recently, many researchers have made huge efforts to design accurate and reliable automatic methods for the detection of mitoses from Haematoxylin and Eosin (H&E)-stained BC histopathology images. However, the problem of automatic mitosis detection has yet to be solved, due to several challenges that can be summarized as follows:

(1) The appearance of each histology image is strongly affected by the preparation, staining and scanning procedures, and this can have various impacts. For instance, variations in the staining conditions of the histopathology images can also affect the colour intensity of both the histopathology images themselves and the mitotic figures, which makes their detection more complicated;

(2) The mitosis shapes, sizes, and textural configurations are completely different in each of the four growth phases (i.e., prophase, metaphase, anaphase, and telophase), as shown in Figure 1(a). For instance, in the telophase, the nucleus completely divides into two distinct parts, forming new daughter cells, and the cell in this stage is often miscounted as two separate cells, rather than a single cell;

(3) Many other objects that appear in H&E-stained BC tissue biopsies, such as apoptotic, necrotic, compressed or lymphocyte nuclei and junk particles, may also have a similar hyperchromatic appearance to that of the mitotic cells, as shown in Figure 1(b). These non-mitotic mimic cells are generally difficult to distinguish from mitotic cells, even for a trained expert pathologist;

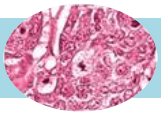

Toward accurate deep learning-based mitosis detection in breast cancer histopathology images

Meriem Sebai. Computer Science Faculty, Algeria
Xinggang Wang, Tianjiang Wang. Huazhong University of Science and Technology (HUST), Wuhan, People's Republic of China
S.A. Al-Fadhli. Imam Al-Kadhum College (IKC), Baghdad, Iraq

(4) The main challenge in the automatic detection of mitoses is their very low density in the HPF image. In fact, mitosis is a very rare event, and this makes the task of mitosis detection more difficult due to the issue of class imbalance, in which the non-mitosis class is strongly dominant compared to the mitosis class.

In the mitosis detection task, only a few benchmarks provide pixel-level annotations of the mitosis regions (for example ICPR12 MITOSIS dataset [7]), and the majority of the mitosis detection benchmarks provide only the annotation of the mitosis centroid pixel (for instance ICPR14 MITOSIS dataset [8]). For CNN-based mitosis detection methods that involve mitosis segmentation, it is preferable to have the annotation of every mitosis pixel in the images (i.e., mitosis pixel-level annotations) to attain full supervision information to train such methods. Hence, with the availability of only mitosis centroid labels in the mitosis detection benchmarks, the segmentation-based methods have to be able to learn with weak labels (i.e., weak supervision). Therefore, the main problem of this research is: **How to perform accurate automatic mitosis detection with weak labels**?

2. Methods

2.1. MaskMitosis: A deep learning framework for fully supervised, weakly supervised, and unsupervised mitosis detection in histopathology images [9]

The main contributions of the proposed MaskMitosis framework can be summarized as follows:

- We propose an adaptation of the general instance segmentation network in natural images Mask RCNN [10] to the task of mitosis detection in histopathology images;
- We propose an effective weakly supervised learning approach that tackles the problem of training our instance segmentation network for mitosis detection on a centroid-pixel annotated dataset. This is based on learning with mitosis pseudo mask labels, which are automatically generated from the mitosis centroid annotations;
- We propose a novel data-based deep transfer learning strategy, which consists of exploiting the multi-task learning of the mitosis instance segmentation model trained in a fully supervised way on a strongly annotated dataset, for the segmentation of the centroid-pixel annotated mitoses ground truth on the weakly labelled dataset, and hence the generation of the mitosis pseudo mask labels;

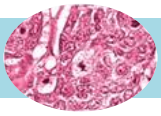

Toward accurate deep learning-based mitosis detection in breast cancer histopathology images

Meriem Sebai. Computer Science Faculty, Algeria
Xinggang Wang , Tianjiang Wang. Huazhong University of Science and Technology (HUST), Wuhan, People's Republic of China
S. A. Al-Fadhli. Imam Al-Kadhum College (IKC), Baghdad, Iraq

- Following the same data-based deep transfer learning strategy but without the guidance of any kind of mitosis annotations, pseudo mask labels are also generated for an unlabelled dataset, which allows to train our instance segmentation network for mitosis detection in an unsupervised way;
- Compared to the existing methods based on classification, regression or object detection, by applying the proposed framework, we improve the mitosis detection accuracy on both pixel-level and centroid-pixel annotated mitosis datasets, and demonstrate the possibility of mitosis detection on an unlabelled mitosis dataset.

The proposed MaskMitosis framework consists of a single network that is used for multiple tasks, as follows: the detection of mitotic cells to enable mitosis counting on datasets with the original pixel-level annotations or estimated pseudo pixel-level annotations, and the segmentation of the mitotic cells for the generation of pseudo pixel-level labels on weakly annotated and unlabelled datasets.

2.1.1 Application of MaskMitosis to mitosis detection

The architecture of the proposed MaskMitosis framework, an adaptive Mask RCNN for mitosis detection and instance segmentation, is shown in Figure 2. MaskMitosis consists of multiple components, and the first of these is the backbone of the network, which is used for feature extraction. This is based on ResNet and a feature pyramid network (FPN). The choice of ResNet-FPN was made because it has achieved excellent performance results as part of numerous methods that have used Mask RCNN to tackle medical tasks. The FPN extends the ResNet architecture (considered as a bottom-up pathway) with a symmetric top-down pathway, and uses skip connections between them to construct an in-network feature pyramid. The skip connections combine the up-sampled feature maps of the top-down pathway with feature maps with similar resolution computed by the last residual block of each ResNet stage from the bottom-up pathway. In this way, the FPN generates multi-scale feature maps by processing a single-scale input image. The second component of our model is the region proposal network (RPN), which applies a sliding sub-network at each location over the multi-level feature maps to generate object proposals with multiple scales and aspect ratios. Each object proposal is described by an anchor, which is a reference box with a specific scale and aspect ratio. The sliding sub-network consists of a convolution (Conv) layer with a 3×3 kernel, which is connected to two sibling FC layers that are used for proposal objectness scoring and prediction of the bounding box positions. Each anchor scale has a corresponding level in the feature pyramid. The RPN used in Mask RCNN has a total of 15 anchors, corresponding to five scales with areas of {322, 642, 1282, 2562, 5122} pixels, and three aspect ratios {1:1, 1:2, 2:1} for each anchor scale. In our system, we apply the default configuration RPN anchors to ensure that we capture all mitotic cells, with different shapes and sizes. The third component is the bounding box recognition and mask prediction network, which exploits the ROIAlign layer to extract a vector of features for each object proposal.

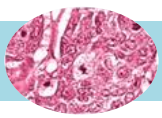

Toward accurate deep learning-based mitosis detection in breast cancer histopathology images

Meriem Sebai. Computer Science Faculty, Algeria
Xinggang Wang, Tianjiang Wang. Huazhong University of Science and Technology (HUST), Wuhan, People's Republic of China
S. A. Al-Fadhli. Imam Al-Kadhum College (IKC), Baghdad, Iraq

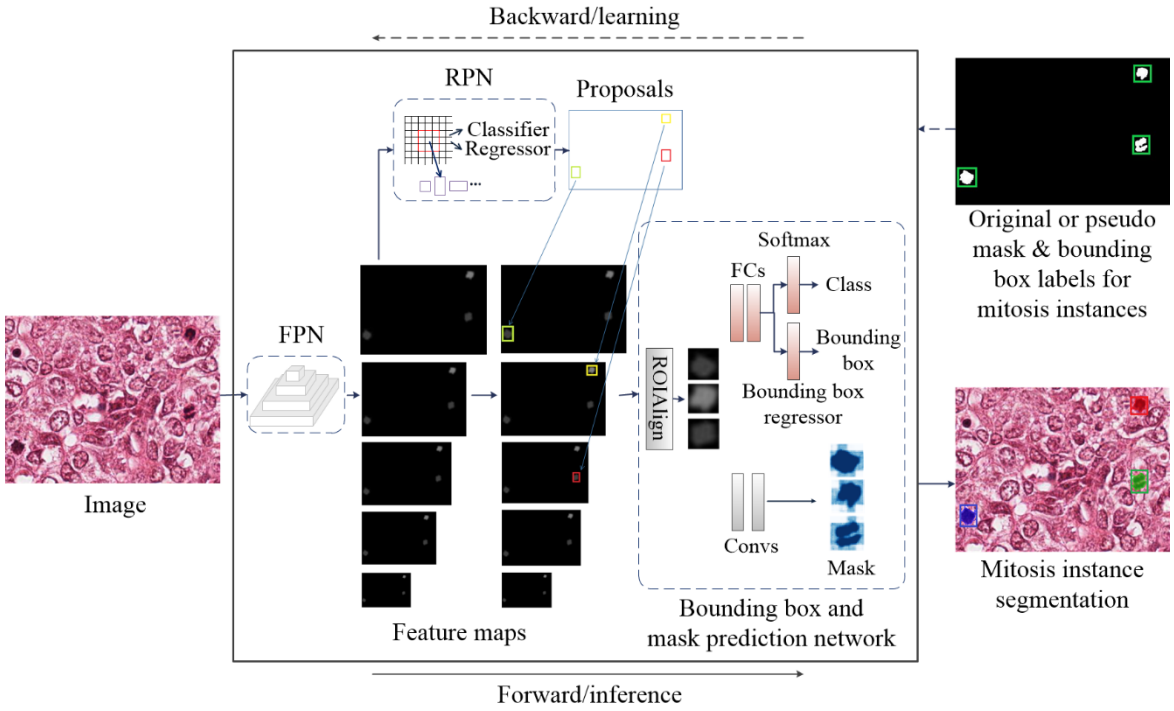

Figure 2. Overview of the proposed MaskMitosis framework [9].

The use of ROIAlign guarantees a precise pixel-to-pixel alignment between the input and the extracted features, which is essential for prediction of the object segmentation mask. The feature patch of each proposal is extracted at a specific level from the feature pyramid, which is selected based on the proposal size. The features of the proposal are then fed into two sub-networks. The first of these sub-networks consists of a set of FC layers followed by two parallel prediction layers: a Softmax layer for object class probability prediction, and a regression layer for refined object bounding box estimation. The second sub-network is a small FCN for object mask prediction. The segmentation branch is trained in parallel with the classification and regression branch.

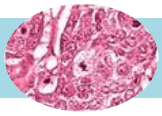

Toward accurate deep learning-based mitosis detection in breast cancer histopathology images

Meriem Sebai. Computer Science Faculty, Algeria
Xinggang Wang , Tianjiang Wang. Huazhong University of Science and Technology (HUST), Wuhan, People's Republic of China
S. A. Al-Fadhli. Imam Al-Kadhum College (IKC), Baghdad, Iraq

Mask RCNN was originally proposed for common object detection and instance segmentation in natural images. Since the size of a mitotic cell is very small, in MaskMitosis framework, we adapt Mask RCNN to make it suitable for mitosis detection by doubling the size of each input image.
MaskMitosis is trained in an end-to-end fashion, with two images per mini-batch. For RPN training, we use an anchor batch of size 256. An object or non-object label is attached to each anchor based on its ratio of overlap with the ground truth bounding boxes. An anchor with a positive label has an intersection-over-union (IoU) of higher than 0.7 with a ground truth box, while an anchor with a negative label has an IoU of less than 0.3 with all ground truth boxes. The remaining anchors (i.e., those with an IoU within the interval [0.3, 0.7]) are discarded during training.

To train the bounding box recognition and mask prediction network, a foreground label is assigned to an object proposal that has an IoU equal or greater than 0.5 with a ground truth box. Meanwhile, 33% of the total number of image ROIs are sampled from these foreground proposals. An object proposal is considered to be background if it has an IoU within the interval [0.1, 0.5) with any ground truth box, and the remaining image ROIs are selected from these background proposals. Mask RCNN uses a ROI batch size of 512. However, due to the low number of mitotic cells in the HPF image, the RPN is generally unable to generate sufficient positive proposals to consistently maintain the 1:3 foreground/background ratio of sampled ROIs per image when the RPN non-maximum suppression (NMS) threshold is 0.7. To fix this issue, we set the RPN NMS threshold to a higher value of 0.9, in order to retain the maximum number of positive proposals.
The task of mitosis detection and counting in histopathology images depends on the number of the correctly detected mitotic cells in each HPF, and does not require a description of the shapes of the mitoses. Hence, at the detection stage, following the detection and instance segmentation of mitotic cells using the MaskMitosis model, we produce a segmentation map of the whole input image and then estimate the mitosis centroid for each segmented blob. These generated mitosis centroids are finally used for evaluation.

2.1.2 Application of MaskMitosis to the estimation of mitosis pseudo mask and bounding box labels on a weakly annotated dataset

The manual annotation of each pixel as mitotic or non-mitotic in histopathology images is a laborious and tedious task. For this reason, most mitosis datasets do not provide pixel-level annotations, and only the mitosis centroid pixel is marked. However, this kind of annotation is inadequate for training the proposed mitosis detection and instance segmentation network, which requires mitosis mask and bounding box labels.

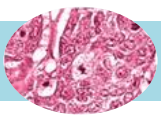

Toward accurate deep learning-based mitosis detection in breast cancer histopathology images

Meriem Sebai. Computer Science Faculty, Algeria
Xinggang Wang, Tianjiang Wang. Huazhong University of Science and Technology (HUST), Wuhan, People's Republic of China
S. A. Al-Fadhli. Imam Al-Kadhum College (IKC), Baghdad, Iraq

To deal with this issue, we use the multi-task learning aspect of MaskMitosis, which combines object detection and object segmentation tasks in one framework, and exploit the segmentation branch of this network to segment the centroid-annotated mitotic cells. The segmentation branch consists of a small FCN that estimates the spatial distribution of the mitosis in each region proposal.
The application of MaskMitosis to the segmentation of mitosis ground truths in a weakly labelled dataset is illustrated in Figure 3. We first train a MaskMitosis model using a pixel-level labelled dataset (ICPR12 MITOSIS dataset), and then use the learned weights to segment the images in the training set of the weakly annotated dataset (ICPR14 MITOSIS dataset). From these predicted mitosis regions, we identify those with a segmented blob that envelops a mitosis centroid label. These segmented mitotic blobs are finally used to generate the pseudo mask and the bounding box labels for each mitosis ground truth. The remaining segmented regions that do not correspond to any annotated mitosis centroid are not taken into consideration.

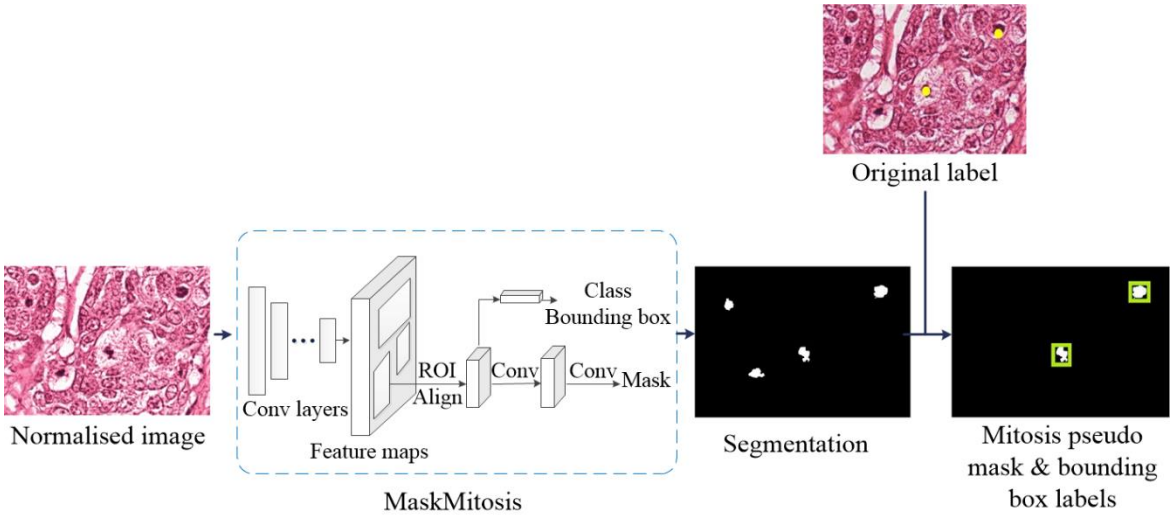

Figure 3 Estimation of the mitosis pseudo mask and bounding box labels for the weakly annotated dataset (ICPR14 MITOSIS dataset), using the MaskMitosis model pretrained on the pixel-level annotated dataset (ICPR12 MITOSIS dataset) [9].

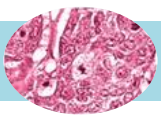

Toward accurate deep learning-based mitosis detection in breast cancer histopathology images

Meriem Sebai. Computer Science Faculty, Algeria
Xinggang Wang , Tianjiang Wang. Huazhong University of Science and Technology (HUST), Wuhan, People's Republic of China
S. A. Al-Fadhli. Imam Al-Kadhum College (IKC), Baghdad, Iraq

Many mitosis regions are not captured by the MaskMitosis model at the segmentation stage due to the variety in the colour intensities of H&E-stained images between the different datasets. The lack of standardisation in terms of dyeing and acquisition procedures of H&E-stained slides between histology laboratories accentuates the inconsistencies in colour across histopathology images. To handle this problem, we perform stain normalisation of the histopathology images in the weakly annotated dataset before estimating the mitosis mask and bounding box labels. This sets the H&E stain colour space of the training images on the weakly annotated dataset to the same as that of the strongly annotated dataset. To achieve this, we apply the widely used Macenko stain normalisation method [11], which is based on stain separation. In this method, it is assumed that each of the two colour stains (i.e., haematoxylin and eosin) in the H&E-stained histopathology image has a corresponding specific stain vector, and the colour of each pixel in the optical density (OD) of the RGB colour space is defined as a linear combination of these two stain vectors. A singular value decomposition (SVD)-based method is then applied to extract these two stain vectors. In order to ensure that all images have the same stain colour space, the obtained stain vectors are used to project the images of interest (here, the images in the weakly annotated training set) onto a reference image (in this case, an image from the strongly annotated dataset) as shown in Figure 4.

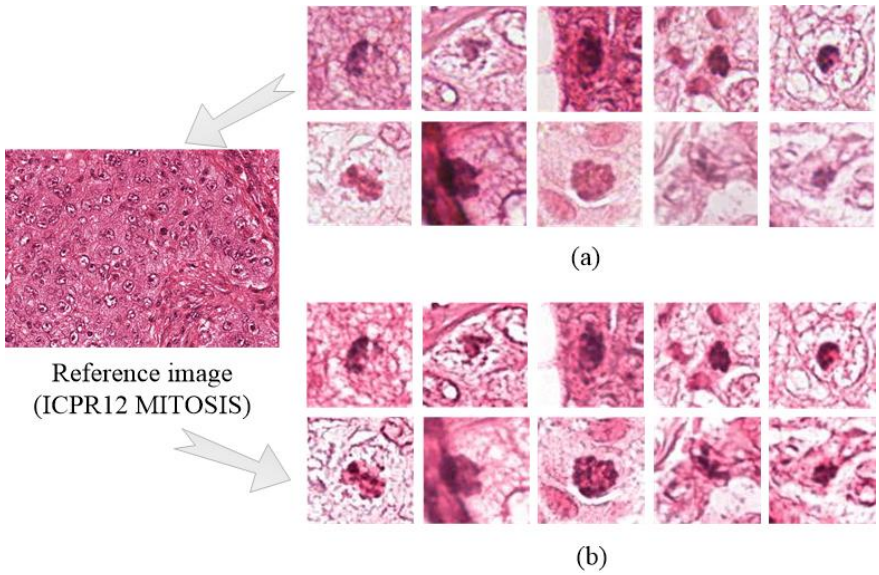

Figure 4. Examples of mitoses from the ICPR14 MITOSIS training set, which the MaskMitosis model pretrained on the ICPR12 MITOSIS dataset failed to segment without stain normalization: (a) mitosis regions without normalization; (b) mitosis regions after normalization [9].

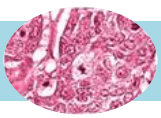

Toward accurate deep learning-based mitosis detection in breast cancer histopathology images

Meriem Sebai. Computer Science Faculty, Algeria
Xinggang Wang , Tianjiang Wang. Huazhong University of Science and Technology (HUST), Wuhan, People's Republic of China
S. A. Al-Fadhli. Imam Al-Kadhum College (IKC), Baghdad, Iraq

After stain normalisation, only a few of the annotated mitosis centroids have no matching segmented region. These mitotic cells are segmented using the Chan-Vese active contour method after transforming the RGB histopathological image into a BR image to intensify the nuclear stain [12] using Equation 1:

$$BR = \frac{(100 \times B)}{(1+R+G)} \times \frac{256}{(1+B+R+G)} \qquad (1)$$

Where B, R, and G are the blue, red, and green channels of the RGB colour space, respectively.

2.1.3 Application of MaskMitosis to the estimation of mitosis pseudo mask and bounding box labels on an unlabelled dataset

Although the weakly supervised learning method can help to considerably minimise the annotation effort required from pathologists, human labour is still required. We therefore propose a MaskMitosis network that learns in an unsupervised way using an unlabelled mitosis dataset. The first step in this learning strategy is to generate mitosis pseudo labels for the training images in this unlabelled dataset, using the MaskMitosis model trained on the strongly annotated dataset.
In the same way as for the estimation of the mitosis pseudo mask and bounding box labels on the weakly annotated dataset, we first apply stain normalisation to the histopathological images in the training set of the unlabelled dataset, and then apply the MaskMitosis model trained on the pixel-level annotated dataset to segment the mitosis regions in these images. Unlike the strongly and weakly annotated mitosis datasets, the unlabelled dataset provides no labels or information about the mitosis ground truths. All of the mitosis regions segmented by the MaskMitosis model trained using a fully supervised approach are therefore used to generate the mitosis pseudo mask and bounding box labels for the unlabelled dataset. The application of MaskMitosis to the segmentation of mitosis ground truths in the unlabelled dataset is illustrated in Figure 5.

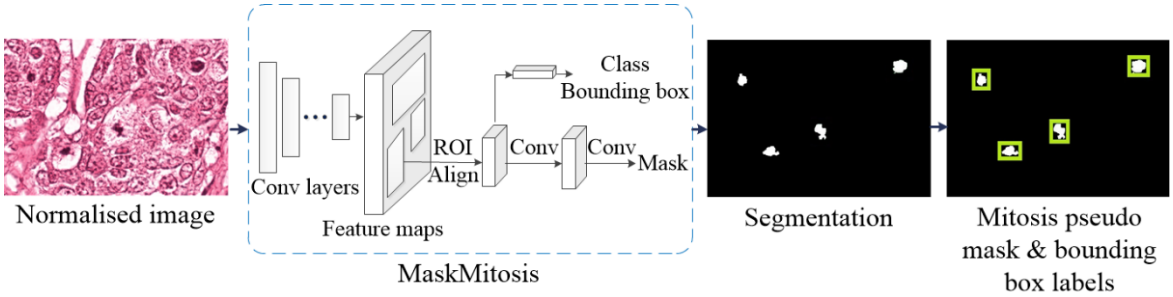

Figure 5. Estimation of the mitosis pseudo mask and bounding box labels for the unlabelled dataset, using the MaskMitosis model trained on the pixel-level annotated dataset [9].

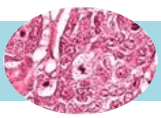

Toward accurate deep learning-based mitosis detection in breast cancer histopathology images

Meriem Sebai. Computer Science Faculty, Algeria
Xinggang Wang, Tianjiang Wang. Huazhong University of Science and Technology (HUST), Wuhan, People's Republic of China
S. A. Al-Fadhli. Imam Al-Kadhum College (IKC), Baghdad, Iraq

To find the most appropriate decision score threshold for the pretrained MaskMitosis model on the ICPR12 MITOSIS dataset that would allow it to retrieve the maximum number of mitosis ground truths for the ICPR14 MITOSIS training set without false detections, we set this threshold to different score values. For each of these values, we trained a MaskMitosis model using estimated mitosis ground truths with a score equal to or higher than this threshold, and then tested this MaskMitosis model on the ICPR14 MITOSIS validation set.

2.1.4 Overview of mitosis detection on strongly and weakly annotated and unlabelled datasets

We utilise two mitosis datasets, ICPR12 MITOSIS [7] and ICPR14 MITOSIS [8], to train and evaluate our MaskMitosis framework. The fully supervised MaskMitosis model is trained and evaluated on the pixel-level annotated ICPR12 MITOSIS dataset, while the weakly supervised model is trained and evaluated on the centroid-pixel annotated ICPR14 MITOSIS dataset. The unsupervised model is trained and evaluated on the ICPR14 MITOSIS dataset, which we treat as an unlabelled dataset by ignoring the mitosis centroid-pixel labels provided with the data.

By exploiting the pixel-level annotations of the ICPR12 MITOSIS dataset, the mitosis mask and bounding box labels can be directly obtained. Hence, the application of MaskMitosis network to the task of mitosis detection on this dataset does not require any prior processing, and training is performed in a fully supervised way. The MaskMitosis model trained on the ICPR12 MITOSIS dataset is called the MaskMitosis12 model, and is illustrated in Figure 6 (a).

Unlike the ICPR12 MITOSIS dataset, which annotates all the pixels of the mitosis regions, ICPR14 MITOSIS only provides the coordinates of the mitosis centroid. A two-step pipeline is therefore required to solve the problem of mitosis detection on this dataset, as shown in Figure 6 (b). In the initial step, we deploy the MaskMitosis12 model to estimate the mitosis pseudo mask and bounding box labels on the training set of ICPR14 MITOSIS. We then retain only those segmented mitosis regions that match the provided mitosis centroid ground truths to generate the mitosis pseudo mask and bounding box labels. In the second step, we use these generated labels to train another MaskMitosis model, called MaskMitosis14, for the detection of mitotic cells on the ICPR14 MITOSIS dataset. In this case, the MaskMitosis14 model is trained in a weakly supervised way.

We also treat ICPR14 MITOSIS as an unlabelled dataset, by ignoring the weak labels provided with the data. In this case, all of the mitosis regions predicted by the MaskMitosis12 model are used to generate the mitosis pseudo mask and bounding box labels. These pseudo labels are then used to train another MaskMitosis14 model in an unsupervised way, as shown in Figure 6 (c).

Figure 5. Estimation of the mitosis pseudo mask and bounding box labels for the unlabelled dataset, using the MaskMitosis model trained on the pixel-level annotated dataset [9].

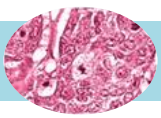

Toward accurate deep learning-based mitosis detection in breast cancer histopathology images

Meriem Sebai. Computer Science Faculty, Algeria
Xinggang Wang , Tianjiang Wang. Huazhong University of Science and Technology (HUST), Wuhan, People's Republic of China
S. A. Al-Fadhli. Imam Al-Kadhum College (IKC), Baghdad, Iraq

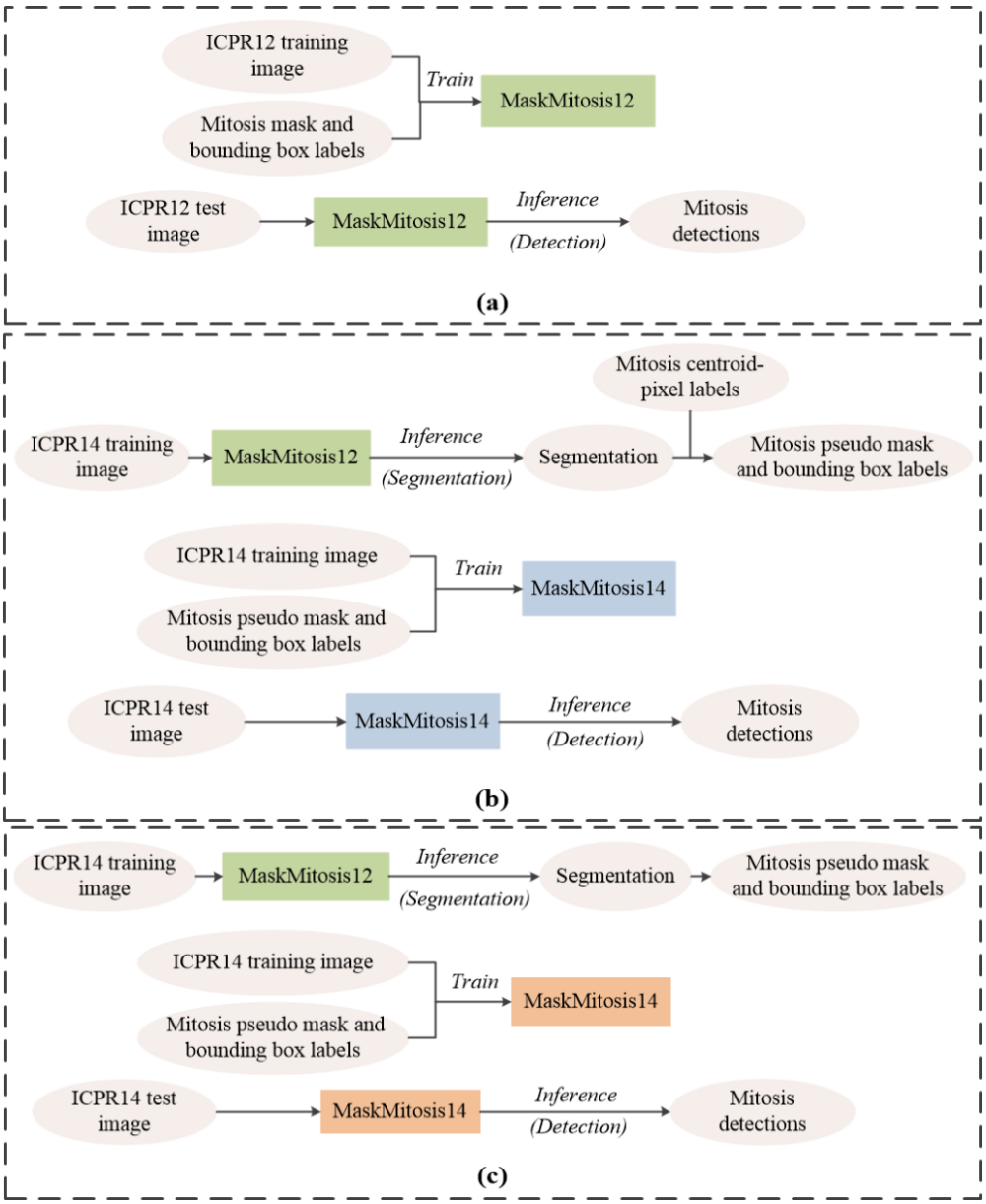

Figure 6. Mitosis detection procedure using fully supervised, weakly supervised and unsupervised learning approaches, with the MaskMitosis framework [9].

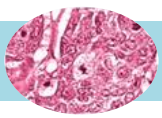

Toward accurate deep learning-based mitosis detection in breast cancer histopathology images

Meriem Sebai. Computer Science Faculty, Algeria
Xinggang Wang , Tianjiang Wang. Huazhong University of Science and Technology (HUST), Wuhan, People's Republic of China
S. A. Al-Fadhli. Imam Al-Kadhum College (IKC), Baghdad, Iraq

2.2 Improved SegMitos Framework for Mitosis Detection in breast cancer histopathology images [13]

The innovative aspects of the proposed iSegMitos framework can be summarised as follows:
- We propose a semantic segmentation framework for mitosis detection, based on an adaptation of the state-of-the-art semantic segmentation network DeepLabv3+ [14]. This framework can perform mitosis detection on pixel-level and centroid-pixel annotated mitosis datasets;
- We propose a robust and effective weakly supervised learning approach that tackles the problem of training the proposed semantic segmentation network on a mitosis centroid-pixel annotated dataset. This approach is based on learning with a novel contextual prior constrained concentric loss function and the corresponding concentric labels;
- Unlike the existing methods for mitosis detection on centroid-pixel annotated dataset, the proposed framework has a high ability to identify the mitotic cells with different sizes, despite their complex appearance configurations.

An illustration of the proposed framework is shown in Figure 7. The DeepLabv3+ network on which the iSegMitos framework is based has a CNN encoder (initially designed for image classification) that employs atrous convolution for dense feature extraction. Unlike image classification networks, which usually have an OS of 32, the encoder has an OS of 16 or 8. This is achieved by removing the striding in the last one or two blocks of the network, for OS of 16 and 8, respectively, and using atrous convolution instead. For instance, for an OS of 8, atrous convolutions with rates of 2 and 4 are used in the last two blocks of the network.

The encoder also employs an ASPP module that can effectively encode semantic information at multiple scales through the use of atrous convolutions with various rates. The feature maps produced by the ASPP are combined with image-level features to integrate global contextual information. In the decoder module, the features produced by the encoder are first up-sampled by a factor of 4 and then concatenated with the low-level features of the encoder with the same spatial dimensions.

A convolution with a 1×1 kernel (1×1 Conv, for brevity) is applied to these features before up-sampling and concatenation, to reduce the number of channels. After concatenation, a few convolutions with a 3×3 kernel are employed to refine the features, and then another up-sampling by a factor of 4 is applied.

The backbone of the iSegMitos framework is based on the state-of-the-art Xception image classification model [15], pre-trained on the ImageNet dataset, to which three modifications are applied to further improve the performance on the semantic segmentation task:

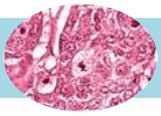

Toward accurate deep learning-based mitosis detection in breast cancer histopathology images

Meriem Sebai. Computer Science Faculty, Algeria
Xinggang Wang , Tianjiang Wang. Huazhong University of Science and Technology (HUST), Wuhan, People's Republic of China
S. A. Al-Fadhli. Imam Al-Kadhum College (IKC), Baghdad, Iraq

- Depth-wise separable convolution with striding is used instead of a max-pooling operation, which helps to significantly increase the network's efficiency. Depth-wise separable convolution involves the factorisation of a regular convolution into a depth-wise convolution and a point-wise convolution. A depth-wise convolution applies a convolution separately on each input channel, and a point-wise convolution aggregates the outputs of the depth-wise convolution over channels.

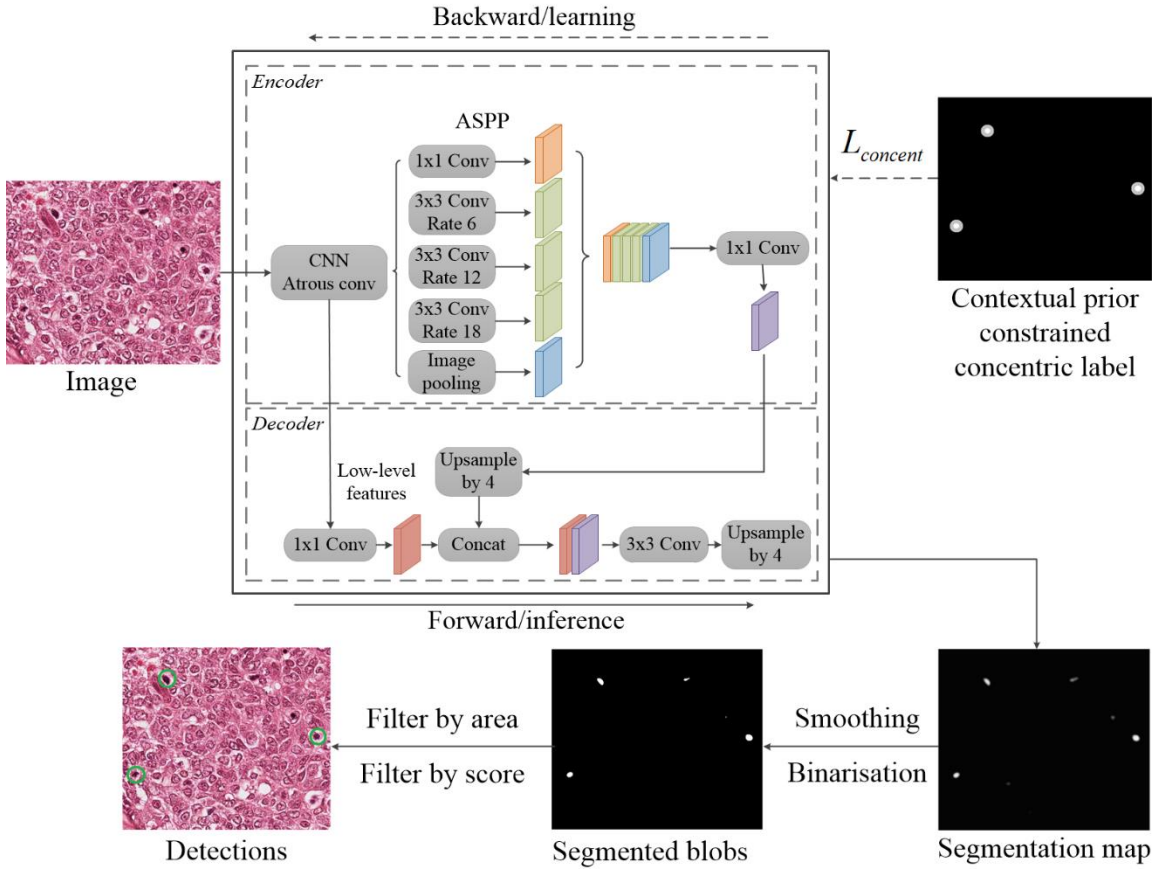

Figure 7 Overview of the iSegMitos framework. Mitosis detections are represented by green circles in the final image [13].

Toward accurate deep learning-based mitosis detection in breast cancer histopathology images

Meriem Sebai. Computer Science Faculty, Algeria
Xinggang Wang , Tianjiang Wang. Huazhong University of Science and Technology (HUST), Wuhan, People's Republic of China
S. A. Al-Fadhli. Imam Al-Kadhum College (IKC), Baghdad, Iraq

A depth-wise separable convolution with striding can be replaced by an atrous separable convolution through the adoption of an atrous convolution in the depth-wise convolution.
- Since the CNN architecture of the Xception model is mainly based on depth-wise separable convolution operations, an extra batch normalisation (BN) and rectified linear unit (ReLU) activation are added to each depth-wise convolution with a 3×3 kernel in the CNN;
- The Xception model consists of three parts: entry flow, middle flow, and exit flow. For semantic segmentation, the depth of the model is increased without modifying the entry flow network structure.

In general, mitosis datasets provide two types of labelling: pixel-level annotation, which provides a mitotic or non-mitotic label for each pixel in the histology image; and centroid-pixel annotation, which annotates only the pixel of the mitosis centroid. Since centroid-pixel annotations are not appropriate for the training of a semantic segmentation network like the iSegMitos network, we transform the centroid-pixel label of each mitosis into a new label that can better define the spatial distribution of the mitosis pixels than the centroid annotation.
Inspired by the contextual prior information of the strongly annotated ICPR12 MITOSIS dataset, we generate a novel kind of label called the concentric label for the centroid-pixel annotated datasets. We choose radius-random circular estimation for each mitotic cell because the intuition that the probability of each surrounding pixel being mitosis is definitely related to the distance between the pixel and the centroid coordinate. Concretely, the concentric label is generated by two random-sized circles, whose centre is located in the annotated centroid coordinate while training.

As illustrated in Figure 8, a concentric label is generated as follows: Around each mitosis centroid, we define two circles: a small circle (shown in yellow in the image in the left of Figure 8) such that all pixels inside of it belong to the mitotic cell, meaning that these pixels will have a mitotic (i.e., positive) label; and a large circle (shown in black in the image in the left of Figure 8) such that all pixels outside of it belong to the background, meaning that they will have a non-mitotic (i.e., negative) label. The small circle is surrounded by an annular region known as the 'middle ground' (shown in grey in the image in the right of Figure 8); this is regarded as a neutral region, since some of its pixels belong to the mitotic cell while others are non-mitotic pixels

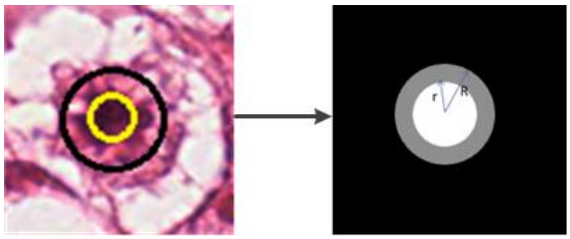

Figure 8. Mitosis contextual prior constrained concentric label [13].

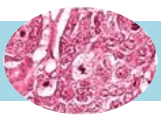

Toward accurate deep learning-based mitosis detection in breast cancer histopathology images

Meriem Sebai. Computer Science Faculty, Algeria
Xinggang Wang , Tianjiang Wang. Huazhong University of Science and Technology (HUST), Wuhan, People's Republic of China
S. A. Al-Fadhli. Imam Al-Kadhum College (IKC), Baghdad, Iraq

The radius of the small and large circles is selected on the basis of the contextual prior information of the area range of mitotic cells from the pixel-level annotated dataset ICPR12 MITOSIS. According to the ICPR12 MITOSIS dataset, the average size of a mitotic cell is about 590 pixels at 40× of magnification. More than 92% of the mitotic cells are within the area range between 230 and 1200 pixels, and over 82% are between 300 and 1200 pixels. The side length statistics of mitotic cells in the ICPR12 MITOSIS dataset are shown in Figure 9. To ensure that the mitosis area in the concentric label includes most of the actual mitosis pixels and excludes the non-mitosis pixels, the small circle is generated randomly within the minimum and median sizes of mitotic cells in the HPF images and the large circle is slightly larger than the maximum area size. Hence, the radius of the small circle r is randomly selected from a uniform distribution within the interval [10, 17], and the radius of the large circle R is randomly set to between 1.5 and 2.5 times the radius of the small circle. We choose this radius range because the statistics in Figure 9 indicate that most of the mitotic cells are with the side lengths larger than 20 (2×10) pixels and rarely is the side length of a mitotic cell more than 85 (2×17×2.5) pixels.

The semantic segmentation network is trained using the contextual prior constrained concentric loss function L_concent, a pixel-wise Softmax loss function in which the pixels contained in the annular region are not used in its computation, as shown in Equation 2:

$$L_{concent} = \sum_{x \in C_1} -log\ \ P(1|x;W) + \sum_{x \in B} -log\ \ P(0|x;W) \qquad (2)$$

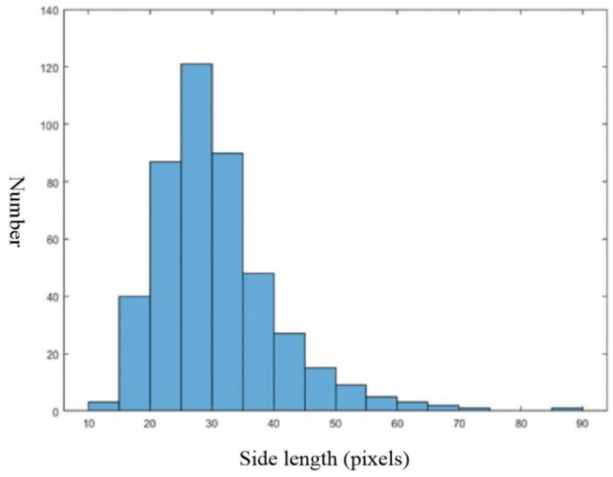

Figure 9. Side length statistics of mitotic cells in the ICPR12 MITOSIS dataset [13].

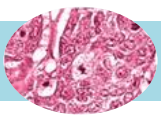

Toward accurate deep learning-based mitosis detection in breast cancer histopathology images

Meriem Sebai. Computer Science Faculty, Algeria
Xinggang Wang , Tianjiang Wang. Huazhong University of Science and Technology (HUST), Wuhan, People's Republic of China
S. A. Al-Fadhli. Imam Al-Kadhum College (IKC), Baghdad, Iraq

Where W are the weights of the network, x is the pixel, and P(1|x;W) is the probability that pixel x is mitotic. C_1 and B represent the mitotic area inside the small circle and the non-mitotic area outside the large circle, respectively. The annular region between B and C_1 is ignored in the computation of the loss function.

In order to train a better semantic segmentation model for mitosis detection in weakly annotated datasets, we propose to transfer the knowledge learned by a model using strong supervision to learn a model with weak supervision, i.e., to carry out mitosis detection in weakly annotated datasets, we fine-tune the iSegMitos network initialised with the weights from the iSegMitos model pre-trained on a strongly annotated dataset.

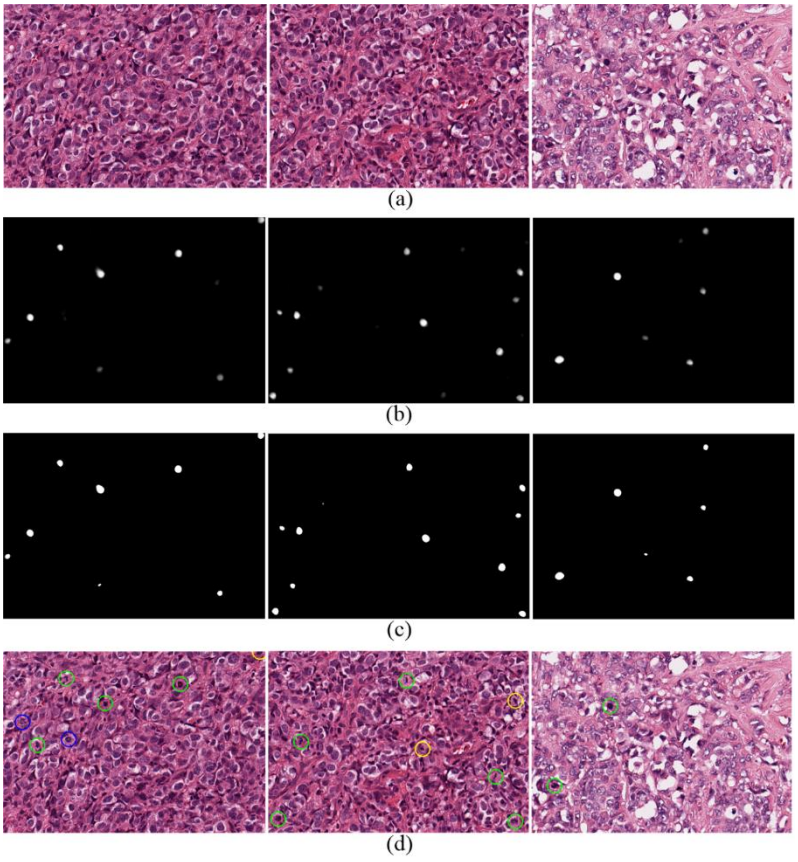

Figure 10. Visual impact of the heuristic method: (a) input images; (b) segmentation maps; (c) segmentation maps after binarisation; (d) mitosis detections after filtering. True positives in green, false negatives in blue, and false positives in yellow [13].

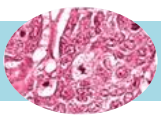

Toward accurate deep learning-based mitosis detection in breast cancer histopathology images

Meriem Sebai. Computer Science Faculty, Algeria
Xinggang Wang , Tianjiang Wang. Huazhong University of Science and Technology (HUST), Wuhan, People's Republic of China
S. A. Al-Fadhli. Imam Al-Kadhum College (IKC), Baghdad, Iraq

At detection time, we use the iSegMitos model trained on the mitosis dataset to segment the H&E-stained slides and predict a pixel-wise segmentation map that gives the probability that each pixel is mitotic. To infer the mitotic cells, we use a heuristic method in which we first smooth the predicted map using a Gaussian filter to eliminate noise and ambiguous particles. To generate the segmented blobs, we binarise the smoothed segmentation map. Otsu's method is applied to determine the binarisation threshold. Finally, since the segmented blobs represent mitosis candidates, we apply a filtering procedure to exclude false mitoses. This filtering procedure combines two features: the area of the blob, and its average probability score. A blob is counted as a true mitosis if its area A is higher than a threshold a1 and its average confidence score $\bar{S}$ is greater than a threshold s1. This filtering method allows us to exclude mitosis mimics more effectively. Figure 10 illustrates the visual impact of each stage of the heuristic method. As we can see in Figure 10 (d), many false detections are removed due to the application of the filtering procedure based on the area and average score of each segmented blob.

2.3. PartMitosis: A partially supervised deep learning framework for mitosis detection in breast cancer histopathology images [16]

The novel contributions of the proposed PartMitosis framework can be summarised as follows:
- We develop a highly precise semantic segmentation-based framework for mitosis detection from centroid-pixel annotated dataset that, in addition to predicting a coarse segmentation map by a semantic segmentation network which learns with weak supervision, can also predicts a precise segmentation map by another semantic segmentation network which learns with strong supervision (i.e., using pixel-level labels). The later network is trained in a partially supervised way on a large centroid-pixel annotated mitosis dataset in which only a few samples have pixel-level annotations.
- We develop a novel intra-model deep transfer learning strategy by designing and integrating a weight transfer function into the framework. This weight transfer function enables the partially supervised learning in the mitosis detection framework;
- Unlike the other existing semantic segmentation-based frameworks for mitosis detection on centroid-pixel annotated dataset, the proposed framework has a high ability to discriminate between mitotic cells and non-mitotic mimic cells, thanks to the precise information about the shape and appearance of the mitoses learned by the partially supervised semantic segmentation network.

An overview of the proposed PartMitosis framework is shown in Figure 11. It consists of two main components: two semantic segmentation networks, the first of which is a semantic segmentation network, trained with weak labels, and the second is another semantic segmentation network, trained with strong labels; and a weight transfer function that connects the two networks and transfers the semantic knowledge from the first network to the second, thus allowing for the prediction of a segmentation map by the strong segmentation network for all images, including those from the dataset without strong annotations in the training stage.

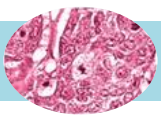

Toward accurate deep learning-based mitosis detection in breast cancer histopathology images

Meriem Sebai. Computer Science Faculty, Algeria
Xinggang Wang, Tianjiang Wang. Huazhong University of Science and Technology (HUST), Wuhan, People's Republic of China
S. A. Al-Fadhli. Imam Al-Kadhum College (IKC), Baghdad, Iraq

Let C be the set of training data that we use to train PartMitosis model. The existing methods presume that all training samples in C are annotated either with a mitosis centroid-pixel label or with a pixel-level label. We presume that C=A∪B, where samples from the set A have pixel-level labels and thus also have centroid-pixel labels (since we can easily extract a centroid label from pixel-level labels), while samples from the set B have only centroid pixel labels.

The ICPR12 MITOSIS dataset is strongly annotated while the ICPR14 MITOSIS dataset is weakly annotated. Since the training of PartMitosis requires both types of mitosis annotations (i.e., pixel-level and centroid-pixel annotations), to train a PartMitosis model for mitosis detection in the ICPR14 MITOSIS dataset, we use the samples of this dataset as set B and use the samples of the ICPR12 MITOSIS dataset as set A.

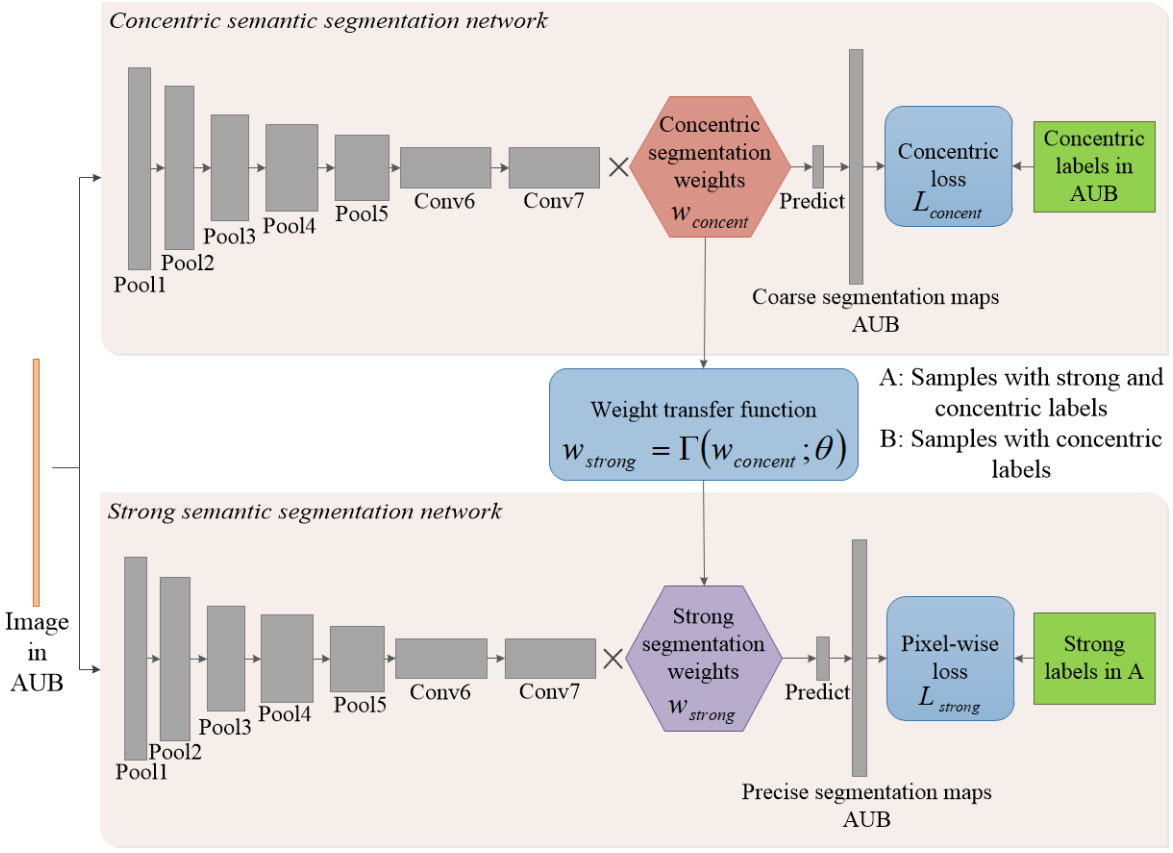

Figure 11. Overview of the proposed PartMitosis framework [16].

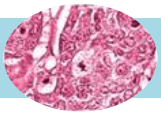

Toward accurate deep learning-based mitosis detection in breast cancer histopathology images

Meriem Sebai. Computer Science Faculty, Algeria
Xinggang Wang , Tianjiang Wang. Huazhong University of Science and Technology (HUST), Wuhan, People's Republic of China
S. A. Al-Fadhli. Imam Al-Kadhum College (IKC), Baghdad, Iraq

Each of the deep semantic segmentation networks in PartMitosis is based on an FCN. An FCN [17] is a dense prediction CNN used for semantic segmentation in natural images. It extends a deep classification network to input images of arbitrary sizes, and outputs a segmentation map of the corresponding size by transforming the FC layers into convolution layers followed by an up-sampling layer. The FCN is pre-trained using image classification task and then fully convolutionally fine-tuned for a fast dense learning and accurate dense prediction.

The spatial precision of the output of the FCN depends on the stride in its last convolutional layer before up-sampling, where a larger stride gives a coarser prediction map. In general, the stride of the prediction layer of the FCN is 32 pixels. However, the spatial resolution of the predicted output can be refined (i.e., made more precise) through a hierarchical combination of the feature maps of the lower layers, which have finer strides and smaller receptive fields, with the original prediction map. This hierarchical combination is performed using skip connections, and allows us to exploit the complementary information in the different prediction layers at multiple levels.

The FCN-32s is the most suitable semantic segmentation network for PartMitosis framework for many reasons: due to the simple structure of the FCN-32s, we can easily fit two FCN-32s into a single GPU without occupying too much memory; the integration of the weight transfer function into our framework that uses two FCN-32s is very simple and straightforward; and the FCN-32s is a semantic segmentation network that can achieve an excellent trade-off between accuracy and speed.

The FCN is a simple yet effective deep learning network originally designed for semantic segmentation in natural images. Much previous research has shown the advantages of knowledge transfer from the domain of natural images to the domain of medical images. Hence, for both networks, we propose using an FCN-32s model pre-trained on natural images as the initial model and fine-tuning it on the mitosis detection datasets to achieve more accurate semantic segmentation performance.

The first semantic segmentation network is the weakly supervised semantic segmentation network that we called the concentric segmentation network. It is trained using the samples from the centroid-pixel annotated dataset B and the samples from the pixel-level annotated dataset A after converting the pixel-level labels into centroid-pixel labels. Since a centroid label is inappropriate for training a deep semantic segmentation network because it does not provide any information about the spatial distribution of the mitosis, we propose transforming the centroid-pixel label of a mitosis into the contextual prior constrained concentric label proposed in the preceding method. The concentric segmentation network is trained with the contextual prior constrained concentric loss function.

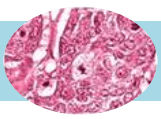

Toward accurate deep learning-based mitosis detection in breast cancer histopathology images

Meriem Sebai. Computer Science Faculty, Algeria
Xinggang Wang , Tianjiang Wang. Huazhong University of Science and Technology (HUST), Wuhan, People's Republic of China
S. A. Al-Fadhli. Imam Al-Kadhum College (IKC), Baghdad, Iraq

The second semantic segmentation network, referred to as the strong segmentation network, is trained in a partially supervised way with the pixel-wise Softmax loss function using the pixel-level labels of the strongly annotated dataset A.
Since the last convolutional layer of the concentric segmentation network and the last convolutional layer of the strong segmentation network both contain semantic parameters, we propose predicting the semantic parameters of the strong segmentation network from the semantic parameters of the concentric segmentation network rather than training them separately. This kind of intra-model deep transfer learning is performed through a weight transfer function. The whole framework, which comprises the two segmentation networks and the weight transfer function, is trained jointly in an end-to-end manner.

Let $W_{concent}$ be the weights of the last convolutional layer (i.e., the prediction layer) before the up-sampling of the FCN trained with the concentric labels, and let W_{strong} be the weights of the last convolutional layer of the FCN trained with the strong labels. A weight prediction function Γ(.) is used to parameterise W_{strong}, rather than considering W_{strong} as model's parameters (see Equation 3 to 5).

$$Predict_{concent} = Conv(output7_{concent}; W_{concent}) \quad (3)$$

Here, Conv(.) means an operation of convolution. $Predict_{concent}$ are the predictions of the last convolutional layer (i.e., the prediction layer) before the up-sampling of the concentric FCN, while $output7_{concent}$ is the output of the previous convolution layer (i.e., Conv7) of the concentric FCN. $W_{concent}$ are learned parameters of the prediction layer of the concentric FCN.

$$W_{strong} = \Gamma(W_{concent}; \theta) \quad (4)$$

Here, θ are learned parameters of the weight transfer function Γ(.) that takes as input $W_{concent}$ and outputs W_{strong}.

$$Predict_{strong} = Conv(output7_{strong}; W_{strong}) \quad (5)$$

Here $Predict_{strong}$ are the predictions of the last convolutional layer (i.e., the prediction layer) before the up-sampling of the strong FCN, while $output7_{strong}$ is the output of the previous convolution layer (i.e., Conv7) of the strong FCN. W_{strong} are the parameters of the prediction layer of the strong FCN, which are not learned but predicted by the weight transfer function Γ(.).

We expect that the weight transfer function Γ(.) is able to transfer coarse semantic information about the mitoses in the weakly annotated dataset to the strong segmentation network in order to learn more precise semantic information about these mitotic cells.

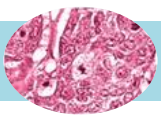

Toward accurate deep learning-based mitosis detection in breast cancer histopathology images

Meriem Sebai. Computer Science Faculty, Algeria
Xinggang Wang, Tianjiang Wang. Huazhong University of Science and Technology (HUST), Wuhan, People's Republic of China
S. A. Al-Fadhli. Imam Al-Kadhum College (IKC), Baghdad, Iraq

We implement Γ(.) using a small fully connected network comprising two FC layers, as illustrated in Figure 12. The FC hidden layer is followed by an activation function of type LeakyReLU. This weight function is used to tackle the problem of the prediction of the strong segmentation map for images from the dataset without strong annotations in the training stage. It helps transfer the semantic information from the weak predictors to the strong predictors. In the training stage, the strong segmentation network and the weight transfer function Γ receive the gradient from the pixel-wise loss computed on set A only, while in the testing stage, a segmentation map can be predicted by the strong segmentation network for all images in set A∪B.

2.3.1. Model training

We train the concentric segmentation network using the two-class contextual prior constrained concentric loss function $L_{concent}$ on the set C=A∪B, and we train the strong segmentation network and the weight transfer function Γ(.) using a two-class pixel-wise Softmax loss function L_{strong} on the set A only. Thus, the overall loss function L is defined as (Equation 6):

$$L = L_{concent} + L_{strong} \quad (6)$$

Much of the previous literature on different computer vision tasks has shown that the end-to-end training can yield more accurate results than training on each task independently. Thus, we propose to jointly train the concentric segmentation network and the strong segmentation network of the PartMitosis framework in an end-to-end way using the strong and concentric labels of the set A and the concentric labels of the set B. During the training of the network, $W_{concent}$ will receive gradient from the pixel-wise segmentation loss L_{strong} via the weight transfer function Γ(.) only when training with samples from the set A. Hence, directly training the network with backpropagation using the concentric losses on the set A∪B and the pixel-wise losses on the set A may cause an inconsistency in the concentric segmentation weights $W_{concent}$.

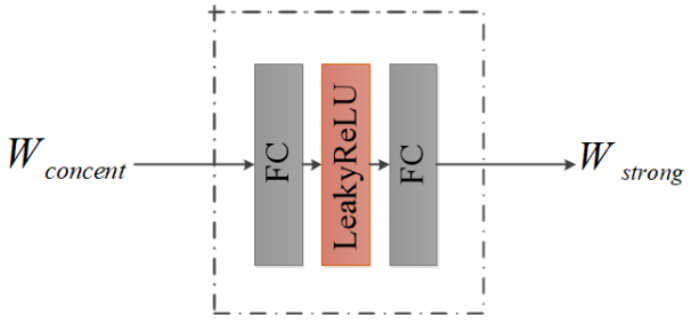

Figure 12. Weight transfer function Γ [16].

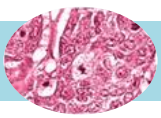

Toward accurate deep learning-based mitosis detection in breast cancer histopathology images

Meriem Sebai. Computer Science Faculty, Algeria
Xinggang Wang , Tianjiang Wang. Huazhong University of Science and Technology (HUST), Wuhan, People's Republic of China
S. A. Al-Fadhli. Imam Al-Kadhum College (IKC), Baghdad, Iraq

Thus, in order to not impede the homogeneity of $W_{concent}$ between the sets A and B, we follow this strategy: when L_{strong} is backpropagated in the network, the gradient of the weight prediction function $\Gamma(W_{concent}; \theta)$ is computed with respect to θ which is the transfer function parameter and stopped with respect to $W_{concent}$, so that the gradient will not be backpropagated to $W_{concent}$. This can be implemented as W_{strong}=Γ(stop-grad($W_{concent}$); θ) in most neural network toolkits. Therefore, $W_{concent}$ will be updated on every training iteration using only the gradient coming from $L_{concent}$ no matter whether the training sample used for this iteration is from the set A or the set B.

2.3.2. Model inference

After the training of the PartMitosis model, we apply it to predict two segmentation maps on the BC histological images, as illustrated in Figure 13. The first segmentation map is denoted by $S_{concent}$, and is the segmentation map produced by the concentric segmentation network, while the second segmentation map, denoted by S_{strong} is the segmentation map generated by the strong segmentation network. The segmentation map output by each network contains the probability score of each pixel to be a mitosis. In order to generate the final segmentation map, we fuse the concentric score map $S_{concent}$ and the strong score map S_{strong} using Equation 7.

$$S = w \times S_{concent} + (1 - w) \times S_{strong} \quad (7)$$

We optimize the fusion weight w on the validation set using parameter sweep, i.e., we produce the segmentation maps $S_{concent}$ and S_{strong} for each sample in the validation set, then, for each value of w within the range [0, 1] with a step of 0.1, we produce the fused segmentation maps for all samples in the validation set and then compute the F-score of the model. The weight w that yields the best F-score is used as the model fusion parameter.

The fused prediction map may still contain some noise and tiny ambiguous cells. In order to eliminate them, we propose using the same heuristic method as in the preceding chapter, which consists of smoothing the segmentation map by applying a Gaussian filter and then binarizing the smoothed map using Otsu's method to obtain the segmented blobs. These segmented blobs include mitotic cells as well as some mimic cells. Hence, to filter out the false positives, we eliminate the segmented blobs with an average score $\bar{S}$ less than a threshold s1 or with an area A smaller than a threshold a1; otherwise, the blob will be kept and considered as a true mitotic cell. As for the weight w, the score threshold s1 and the area threshold a1 are also optimized on the validation set.

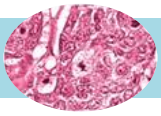

Toward accurate deep learning-based mitosis detection in breast cancer histopathology images

Meriem Sebai. Computer Science Faculty, Algeria
Xinggang Wang, Tianjiang Wang. Huazhong University of Science and Technology (HUST), Wuhan, People's Republic of China
S. A. Al-Fadhli. Imam Al-Kadhum College (IKC), Baghdad, Iraq

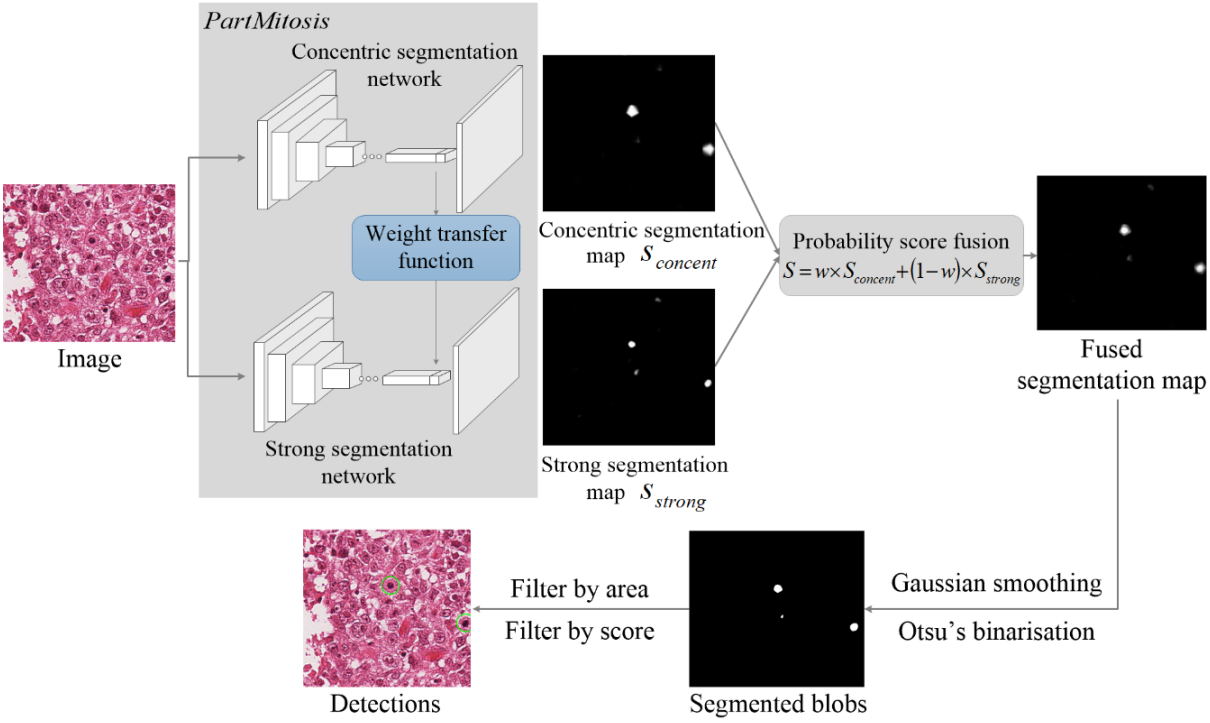

Figure 13. Detection of mitotic cells with the PartMitosis framework. The mitosis detections are represented by the green circles in the final image [16].

3. Experimental results

In this section, we report the results of the experiments carried out to assess the detection performance of the proposed MaskMitosis, iSegMitos, and PartMitosis frameworks on two different mitosis datasets, namely ICPR12 MITOSIS and ICPR14 MITOSIS. We also compare the detection results achieved by the proposed frameworks with state-of-the-art mitosis detection methods.

To evaluate the performance of an automatic mitosis detection method, we use the same measurement criteria as in the mitosis detection challenges. Note that the task of detecting mitoses from BC histopathology slides does not involve describing the shapes of the detected mitotic cells, but instead relies on counting the number of accurately detected mitoses. A detection is considered to be correct if the distance from its centroid to the centroid of a ground truth is within a certain range. This distance range varies from one mitosis dataset to another; for instance, the range is 8 µm (32 pixels) for ICPR14 MITOSIS and 5 µm (20 pixels) for ICPR12 MITOSIS.

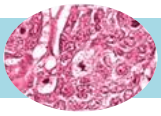

Toward accurate deep learning-based mitosis detection in breast cancer histopathology images

Meriem Sebai. Computer Science Faculty, Algeria
Xinggang Wang, Tianjiang Wang. Huazhong University of Science and Technology (HUST), Wuhan, People's Republic of China
S. A. Al-Fadhli. Imam Al-Kadhum College (IKC), Baghdad, Iraq

There are three metrics that are used to evaluate automatic mitosis detection methods: precision, recall, and the harmonic average of precision and recall, which is referred to as the F-score. These metrics are computed using the following formulae (Equation 8 to 10):

$$precision=TP/(TP+FP) \quad (8)$$

$$recall=TP/(TP+FN) \quad (9)$$

$$F\text{-}score=2\times precision\times recall/(precision+recall) \quad (10)$$

Where TP represents the number of true positives (i.e., the correctly detected mitoses), FN represents the number of false negatives (i.e., mitoses that are not detected), and FP represents the number of false positives (i.e., false mitosis detections).

Table 1 shows the experimental results from the proposed methods and other existing state-of-the-art methods on the ICPR12 MITOSIS testing set. Table 2 shows the F-scores for the proposed approaches on the ICPR14 testing set, as well those of some other approaches. Evaluation experiments showed that the three proposed methods achieved excellent results on the two different mitosis detection datasets.

Method	Precision	Recall	F-score
UDT-CWT [18]	0.710	0.760	0.730
CasNN [19]	0.738	0.753	0.745
E-CNN [20]	0.860	0.690	0.760
SegMitos [21]	0.813	0.732	0.770
MSSN [22]	0.776	0.787	0.781
DRN [23]	0.779	0.802	0.790
TP-CNN [24]	0.830	0.760	0.790
Joint Learning [25]	-	-	0.812
DeepMitosis [26]	0.854	0.812	0.832
Haar-DWT+CNN [27]	0.845	0.837	0.841
Improved RCNN [28]	0.920	0.792	0.851
Attention RCNN [29]	0.883	0.822	0.851
MaskMitosis [9]	0.921	0.811	0.863
iSegMitos [13]	0.851	0.792	0.820
PartMitosis [16]	0.766	0.811	0.788

Table 1 F-scores for the proposed frameworks and other methods on the ICPR12 MITOSIS testing set ("-" denotes an unreported result).

Toward accurate deep learning-based mitosis detection in breast cancer histopathology images

Meriem Sebai. Computer Science Faculty, Algeria
Xinggang Wang , Tianjiang Wang. Huazhong University of Science and Technology (HUST), Wuhan, People's Republic of China
S. A. Al-Fadhli. Imam Al-Kadhum College (IKC), Baghdad, Iraq

Method	Precision	Recall	F-score
Attention RCNN [29]	-	-	0.400
DeepMitosis [26]	0.431	0.443	0.437
CasNN [19]	0.411	0.478	0.442
MSSN [22]	0.379	0.617	0.470
SmallMitosis [30]	0.512	0.479	0.495
Multi-stream Faster RCNN [31]	-	-	0.507
Haar-DWT+CNN [27]	0.544	0.576	0.560
SegMitos [21]	0.637	0.502	0.562
UBCNN [32]	0.485	0.694	0.571
MaskMitosis [9]	0.500	0.453	0.475
iSegMitos [13]	0.601	0.541	0.569
PartMitosis [16]	0.664	0.507	0.575

Table 2 Comparison of the performance of the proposed frameworks with other approaches on the ICPR14 MITOSIS testing set ("-" denotes an unreported result).

References

[1] A. Jemal, F. Bray, M. M. Center, et al. Global cancer statistics. CA: A Cancer Journal for Clinicians, 2011, 61(2):69-90.
[2] E. A. Rakha, J. S. Reis-Filho, F. Baehner, et al. Breast cancer prognostic classification in the molecular era: The role of histological grade. Breast Cancer Research, 2010, 12(4):1-12.
[3] R. B. Greenough. Varying degrees of malignancy in cancer of the breast. The Journal of Cancer Research, 1925, 9(4):453-463.
[4] H. J. G. Bloom and W. W. Richardson. Histological grading and prognosis in breast cancer: A study of 1409 cases of which 359 have been followed for 15 years. British Journal of Cancer, 1957, 11(3):359.
[5] C. W. Elston and I. O. Ellis. Pathological prognostic factors in breast cancer. I. The value of histological grade in breast cancer: Experience from a large study with long-term follow-up. Histopathology, 1991, 19(5):403-410.
[6] R. Gal, L. Rath-Wolfson, Y. Rosenblatt, et al. An improved technique for mitosis counting. International Journal of Surgical Pathology, 2005, 13(2):161-165.
[7] L. Roux, D. Racoceanu, N. Lomenie, et al. Mitosis detection in breast cancer histological images: An ICPR 2012 contest. Journal of Pathology Informatics, 2013, 4:8.

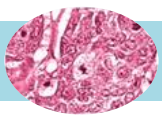

Toward accurate deep learning-based mitosis detection in breast cancer histopathology images

Meriem Sebai. Computer Science Faculty, Algeria
Xinggang Wang , Tianjiang Wang. Huazhong University of Science and Technology (HUST), Wuhan, People's Republic of China
S. A. Al-Fadhli. Imam Al-Kadhum College (IKC), Baghdad, Iraq

[8] L. Roux. Mitosis Atypia 14 Grand Challenge.
[9] M. Sebai, X. Wang, and T. Wang. MaskMitosis: A deep learning framework for fully supervised, weakly supervised, and unsupervised mitosis detection in histopathology images. Medical and Biological Engineering and Computing, 2020, 58:1603-1623.
[10] K. He, G. Gkioxari, P. Dollar, et al. Mask RCNN. 2017 16th IEEE International Conference on Computer Vision (ICCV), Venice, Italy, 2017, pp. 2980-2988.
[11] M. Macenko, M. Niethammer, J. S. Marron, et al. A method for normalizing histology slides for quantitative analysis. 2009 6th IEEE International Symposium on Biomedical Imaging (ISBI), Boston, USA, 2009, pp. 1107-1110.
[12] H. Chang, L. A. Loss, and B. Parvin. Nuclear segmentation in H&E sections via multi-reference graph cut (MRGC). 2012 9th IEEE International Symposium on Biomedical Imaging (ISBI), Barcelona, Spain, 2012, pp.614-617.
[13] M. Sebai. Improved SegMitos framework for mitosis detection in breast cancer histopathology images. 2020 IEEE International Conference on Artificial Intelligence and Information Systems (ICAIIS), Dalian, China, 2020, pp. 102-106.
[14] L. C. Chen, Y. Zhu, G. Papandreou, et al. Encoder-decoder with atrous separable convolution for semantic image segmentation. 2018 15th European Conference on Computer Vision (ECCV), Munich, Germany, 2018, pp. 801-818.
[15] N. Tajbakhsh, J. Y. Shin, S. R. Gurudu, et al. Convolutional neural networks for medical image analysis: Full training or fine tuning?. IEEE Transactions on Medical Imaging, 2016, 35(5):1299-1312.
[16] M. Sebai, T. Wang, and S. A. Al-Fadhli. PartMitosis: A partially supervised deep learning framework for mitosis detection in breast cancer histopathology images. IEEE Access, 2020, 8:45133-45147.
[17] J. Long, E. Shelhamer, and T. Darrell. Fully convolutional networks for semantic segmentation. 2015 28th IEEE Conference on Computer Vision and Pattern Recognition (CVPR), Boston, USA, 2015, pp. 3431-3440.
[18] T. Wan, W. Zhang, M. Zhu, et al. Automated mitosis detection in histopathology based on non-Gaussian modeling of complex wavelet coefficients. Neurocomputing, 2017, 237:291-303.
[19] H. Chen, Q. Dou, X. Wang, et al. Mitosis detection in breast cancer histology images via deep cascaded networks. 2016 30th AAAI Conference on Artificial Intelligence, Phoenix, USA, 2016, pp.1160-1166.
[20] M. Saha, C. Chakraborty, and D. Racoceanu. Efficient deep learning model for mitosis detection using breast histopathology images. Computerized Medical Imaging and Graphics, 2018, 64:29-40.
[21] C. Li, X. Wang, W. Liu, et al. Weakly supervised mitosis detection in breast histopathology images using concentric loss. Medical Image Analysis, 2019, 53:165-178.
[22] M. Ma, Y. Shi, W. Li, et al. A novel two-stage deep method for mitosis detection in breast cancer histology images. 2018 24th International Conference on Pattern Recognition (ICPR), Beijing, China, 2018, pp. 3892-3897.
[23] H. Chen, X. Wang, and P. A. Heng. Automated mitosis detection with deep regression networks. 2016 13th IEEE International Symposium on Biomedical Imaging (ISBI), Prague, Czech Republic, 2016, pp. 1204-1207.
[24] N. Wahab, A. Khan, and Y. S. Lee. Two-phase deep convolutional neural network for reducing class skewness in histopathological images based breast cancer detection. Computers in Biology and Medicine, 2017, 85:86-97.
[25] P. Pati, A. Foncubierta-Rodriguez, O. Goksel, et al. Mitosis detection under limited annotation: A joint learning approach. 2020 17th IEEE International Symposium on Biomedical Imaging (ISBI), Iowa City, USA, 2020, pp. 486-489.

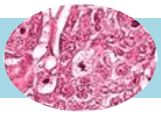

Toward accurate deep learning-based mitosis detection in breast cancer histopathology images

Meriem Sebai. Computer Science Faculty, Algeria
Xinggang Wang , Tianjiang Wang. Huazhong University of Science and Technology (HUST), Wuhan, People's Republic of China
S. A. Al-Fadhli. Imam Al-Kadhum College (IKC), Baghdad, Iraq

[26] C. Li, X. Wang, W. Liu, et al. DeepMitosis: Mitosis detection via deep detection, verification and segmentation networks. Medical Image Analysis, 2018, 45:121-133.
[27] D. K. Das and P. K. Dutta. Efficient automated detection of mitotic cells from breast histological images using deep convolution neural network with wavelet decomposed patches. Computers in Biology and Medicine, 2019, 104:29-42.
[28] H. Lei, S. Liu, H. Xie, et al. An improved object detection method for mitosis detection. 2019 41st Annual International Conference of the IEEE Engineering in Medicine and Biology Society (EMBC), Berlin, Germany, 2019, pp. 130-133.
[29] H. Lei, S. Liu, A. Elazab, et al. Attention-guided multi-branch convolutional neural network for mitosis detection from histopathological images. IEEE Journal of Biomedical and Health Informatics, 2020, 25(2):358-370.
[30] T. Kausar, M. Wang, M. A. Ashraf, et al. SmallMitosis: Small size mitotic cells detection in breast histopathology images. IEEE Access, 2021, 9:905-922.
[31] R. E. Yancey. Multi-stream Faster RCNN for mitosis counting in breast cancer images. ArXiv preprint arXiv:2002.03781, 2020.
[32] X. Lu, Z. You, M. Sun, et al. Breast cancer mitotic cell detection using cascade convolutional neural network with UNet. Mathematical Biosciences and Engineering, 2020, 18(1):673-695.

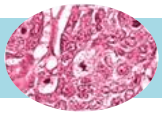

Visual Computing Magazine

Vol 1, Issue 3, 2023

Content